Terr. Atmos. Ocean. Sci., Vol. 30, No. 5, 649-674, Ocober 2019 doi: 10.3319/TAO.2019.07.07.01

# Gas plumes and near-seafloor bottom current speeds of the southernmost Okinawa Trough determined from echo sounders

Ching-Hui Tsai[1], Shu-Kun Hsu[1, 2, *], Yen-Fu Chen[2], Hsiao-Shan Lin[1], Shiou-Ya Wang[1], Song-Chuen Chen[3], Chin-Wei Liang[1], and Yen-Yu Cho[1]

[1] *Center for Environmental Studies, National Central University, Taoyuan City, Taiwan*
[2] *Department of Earth Sciences, National Central University, Taoyuan City, Taiwan*
[3] *Central Geological Survey, Ministry of Economic Affairs, Taipei City, Taiwan*

***Article history:***
Received 26 January 2019
Revised 2 July 2019
Accepted 7 July 2019

***Keywords:***
Gas plume, Bottom current, Okinawa Trough, Echo sounder

***Citation:***
Tsai, C.-H., S.-K. Hsu, Y.-F. Chen, H.-S. Lin, S.-Y. Wang, S.-C. Chen, C.-W. Liang, and Y.-Y. Cho, 2019: Gas plumes and near-seafloor bottom current speeds of the southernmost Okinawa Trough determined from echo sounders. Terr. Atmos. Ocean. Sci., 30, 649-674, doi: 10.3319/TAO.2019.07.07.01

## ABSTRACT

Using echo sounders to detect gas plumes in seawater is common, especially in the context of hydrothermal circulation areas or gas hydrate-bearing cold seeps. To understand the distribution of gas plumes in the southernmost Okinawa Trough, we have conducted 13 cruises with a 38 kHz single-beam echo sounder (EK60). A total of 266 gas plumes of acoustic image, associated with the hydrothermal circulation, are detected. To estimate the near-seafloor bottom current speeds, 201 gas plumes are further used. As a result, the gas plumes around the axial depression of the Okinawa Trough generally tilt to the northeast at rising tides and high tides, suggesting a northeastward flow of the bottom current. However, the gas plumes in the Keelung continental slope tilt to the southwest at ebb tides and low tides, suggesting a southwestward flow of the bottom current. Our results significantly show a good estimation of the near-seafloor bottom currents from EK plume images in the case of lacking real observations. The directions of the bottom currents depend on semi-diurnal tides. Assuming a quasi-constant speed of upward gas bubbles out of seabed, we have estimated the bottom current speeds in 6 hydrothermal circulation zones near the rifting center of the southernmost Okinawa Trough. The estimated bottom current speeds in submarine volcanic areas vary largely from 2 to 160 cm $s^{-1}$, but bottom current speeds in relatively flat region are between 20 and 50 cm $s^{-1}$. The large variation of the bottom current speeds in the submarine volcanic areas could be due to the variable emissions of the gases out of the submarine volcanic areas.

## 1. INTRODUCTION

Relative to the Eurasian Plate, the Philippine Sea Plate moves northwestward at a speed of ~8 cm $yr^{-1}$ around Taiwan (Seno et al. 1993; Yu et al. 1997). The Philippine Sea Plate is subducting beneath the Eurasian Plate and has formed the Ryukyu subduction zone (Letouzey and Kimura 1985; Sibuet et al. 1987). Okinawa Trough is an active back-arc basin behind the Ryukyu Arc (Uyeda 1977; Lee et al. 1980; Kimura 1985; Sibuet et al. 1987) (Fig. 1). Our study area is located in the southernmost Okinawa Trough. Morphologically, Keelung Valley and Mienhua Canyon are loacated in the northern margin of the Okinawa Trough and transport sediments from the East China Sea to the Okinawa Trough (Hsu et al. 1996). The current rifting of the southern Okinawa Trough area could start at 0.1 million years ago (Sibuet et al. 1998).

Kimura et al. (1986, 1988) and Shyu and Liu (2001) have pointed out unusually high geothermal flows in the Okinawa Trough, especially some hydrothermal hillocks and biota. It reveals an actively hydrothermal circulation system in the Okinawa Trough. Earthquakes and active submarine volcanoes are common in the southernmost Okinawa Trough (Lin et al. 2007, 2009). It suggests intensively magma activity associated with abundant submarine volcanoes. Base on the multi-beam bathymetric data from the ACT cruise of the Taiwan-French cooperation in 1996 (Lallemand et al. 1997), there are more than 70 submarine volcanoes in the southernmost area of the Okinawa Trough

* *Corresponding author*
*E-mail: hsu@ncu.edu.tw*

(Fig. 2). Hydrothermal circulations are linked to the activities of the submarine volcanoes (Massoth et al. 1988). In a hydrothermal circulation area, volcanic materials are carried by hot water to form a smoky zone (Baker et al. 1995), creating a "Black Smoker" feature, which provides an important conduit for the exchange of seawater and crustal metals.

Because of a hydrothermal circulation, volcanic material could be carried by hot water and form a relatively turbid area in the seawater. Using a 38 kHz single-beam echo sounder, German et al. (1994) have observed the hydrothermal circulation phenomenon of the mid-ocean ridge in the northeastern Pacific Ocean. Similarly, Tsai (1999) and Lee (2005) also have observed a hydrothermal circulation system in the southernmost of the Okinawa Trough; 12 active hydrothermal areas were discovered (Lee 2005). A 38 kHz single-beam echo sounder has also been used to observe cold seep systems associated with gas hydrates. For example, the researches on gas hydrates in the Black Sea (Polikarpov et al. 1989; Naudts et al. 2006), Hydrate Ridge (Heeschen et al. 2003), and the southwestern Taiwan (Chen et al. 2010; Hsu et al. 2018). However, it is remarkable that several acoustic images of the gas plumes in water columns have been tilted, instead of a vertical ascent. Veloso et al. (2015) used three typical examples of plumes image from single-beam echo sounders to explain how a near-seafloor bottom current could affect rising bubbles from a seabed. The application of multi-beam echo sounder water-column imaging technology allows us to understand the relationship between the shape of the plume shape and the direction of current in the seawater (Urban et al. 2017). Additionally, the mooring observation on the hydrothermal mounds of the mid-ocean ridge (Fujioka et al. 1997) and the ADCP (Acoustic Doppler Current Profiler) observation in the Hatoma Knoll hydrothermal field of the southern Okinawa Trough (Furushima and Yamamoto 2015) have shown that the fluctuation cycle of temperature, pressure, and current is synchronized with semidiurnal tides.

In this study, we will analyze the EK60 acoustic images from 13 surveys in the southernmost Okinawa Trough (Fig. 3), with the purpose of better understanding the gas plumes distribution and the relationship between the gas plumes images and the near-seafloor bottom current in the southernmost Okinawa Trough. As mentioned previously, gas plume locations could be excellent sites for the exchange of seawater and crustal metals; thus, bottom current directions may be used to indicate the probable precipitation areas of metalliferous sediments.

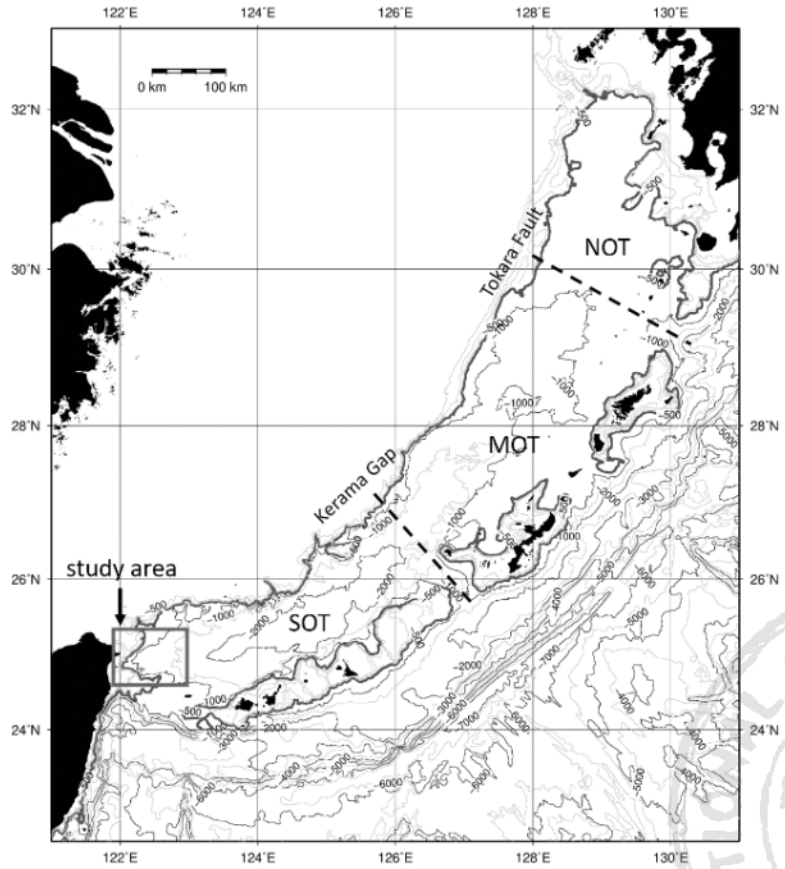


Fig. 1. Bathymetry Bathymetric map of the Okinawa Trough between Taiwan and Japan. The regional map of the Okinawa Trough, which could be separated into three portions. They are the Northern Okinawa Trough (NOT), the Middle Okinawa Trough (MOT), and the Southern Okinawa Trough (SOT), separated by the Kerama Gap and the Tokara Fault respectively. This study area is located in the westernmost OT.

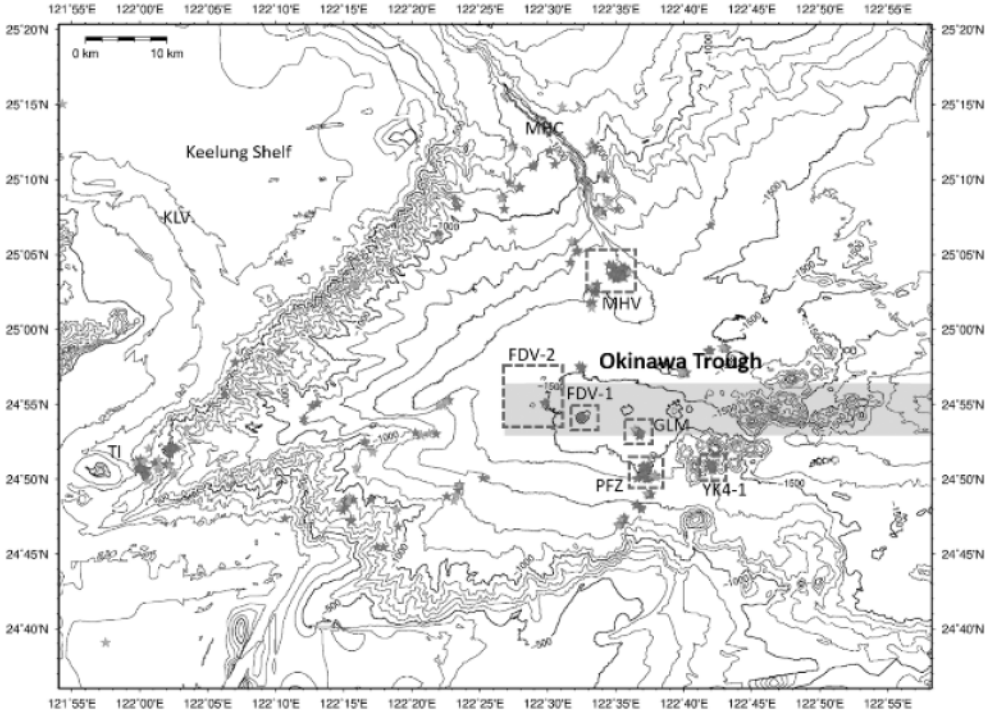


Fig. 2. Topography of the study area. The main features include the southernmost Okinawa Trough back-arc basin, the Keelung Valley (KLV), the Turtle Island (TI), and the Mienhua Canyon (MHC). The stars indicate the locations of the 266 gas plumes. The pink stars indicate the locations of 201 complete plume images and the light blue stars indicate the locations of 65 incomplete gas plume images. The red boxes indicate 6 active hydrothermal circulation zones and 11 gas plume images used to estimate the near-seafloor bottom current velocities. The yellow zone indicates the axial portion of the Okinawa Trough.

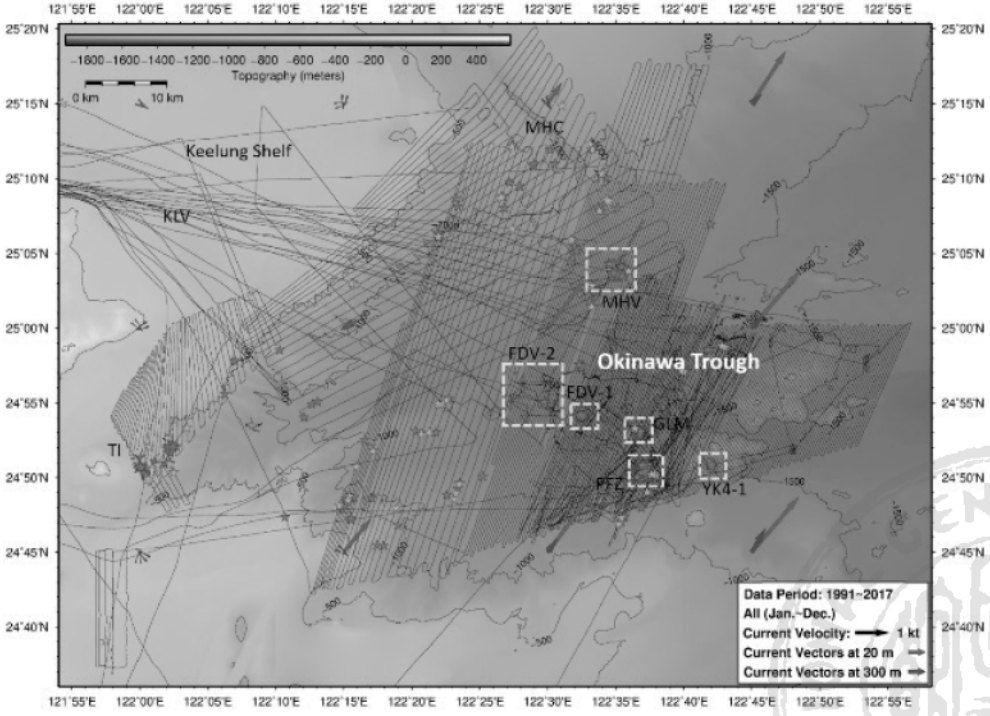


Fig. 3. The ship-tracks of 13 surveys used in this study. The ship-tracks mainly show NE-SW orientation. The data covers the areas of southernmost Okinawa Trough, the Keelung Shelf slope and the northeast side of the Turtle Island. Based on the Ocean Data Bank, the currents at 20 - 300 m deep in the study area are dominated by the northeast flow. The yellow boxes indicate same locations as in Fig. 2.

## 2. DATA COLLECTION AND PROCESSING

The bathymetric data used in this study were collected during 13 cruises from 2014 to 2018 with EK60 scientific single-beam sounder, which uses the split beams technology and two frequencies (38 and 120 kHz). Because the water depths in our study area are generally deeper than 500 m (Fig. 3), we only use the 38 kHz. The transducer has a 7° beam width. Post-processing of data is done with the FM-Midwater tool in the Fledermaus software suite, so that the gas plume images and the adjustment of energy were obtained.

Based on the existing data of physical oceanography for the water depth as deep as 300 m (Ocean Data Bank of the Ministry of Science and Technology, Taiwan, R.O.C.), the annual average current flow has a stable northeast flow in the shallow part to the east of 122°20'E. The current flow becomes faster eastward (Fig. 3). To the west of 122°20'E, morphologically the area belongs to the Keelung continental shelf and slope. It has a slower velocity of flow and inconsistent flow direction; especially the flow direction is quite unstable at a water depth of 300 m (Fig. 3). In any case, there is a lack of current velocity information for the water depths greater than 300 m.

Among our 13 cruises, there are 3 deep-tow sonar surveys with a ship speed of ~2 knots and 10 multi-beam echosounder cruises with a ship speed of ~6 knots. Based on our EK60 data in the southernmost Okinawa Trough, we have identified 266 gas plumes (Figs. 2 and 3 and Appendix A). According to Veloso et al. (2015), the relationship of a gas plume image to a bottom current could have 3 cases: (1) current from the opposite direction of the ship's movement, (2) current from the same direction as the ship's movement, and (3) current oblique to the ship's movement. In the second case, a most complete and clear plume image can be imaged. Because a gas plume image in the third case is obliquely obtained by cutting across the gas plume, the plume image near the seabed is usually missed. In consequence, the portion of the gas plume image could be mistaken for a school of fish in the seawater. Therefore, based on the completeness of our 266 gas plume images, we separated 201 complete images of gas plume (remark A in Appendix A) from 65 incomplete images (remark B in Appendix A). Figures 4 to 16 display the 201 complete images of gas plume that will be further analyzed in this study.

## 3. RESULTS AND DISCUSSION

### 3.1 Gas Plumes and Hydrothermal Circulation

During our 3 deep-tow sonar surveys, sidescan sonar data (120 and 410 kHz) were collected. Active gas plumes (emitting gas bubbles) associated with hydrothermal circulation can be clearly observed in the sidescan sonar images (Figs. 4 and 5). As shown in the sidescan sonar images of Fig. 5, gaseous bubbles or materials carried by hot water have escaped from chimneys or mounds (Hsu 2017). Those gas plumes imaged in the sidescan sonar can also be imaged in the 38 kHz single beam sonar (EK60) (Figs. 4 and 5). The gas plume heights are generally around 350 m, but can be as high as 800 m.

### 3.2 Gas Plumes and Tidal Variation

Crone et al. (2010) indicated that tidal variation could affect current velocity near a hydrothermal vent. Chemical concentrations and temperatures of a current may also be changed (Larson et al. 2007). For example, Veirs et al. (2006) showed that the semi-diurnal tide affects the tidal oscillations of ocean currents around the Grotto mound in the Juan de Fuca Ridge region. Semi-diurnal tides also affect the deep ocean around the mid-Atlantic Ridge (Fujioka and Mitsuzawa 2001) and around the seabed near Oahu of Hawaii (Aucan et al. 2006). In addition, Berdeal (2006) found significant inertial oscillations in the time series of horizontal flow in an 11-month near-bottom ADCP observation; similar result was obtained in the southern Okinawa Trough (Furushima and Yamamoto 2015). It is concluded that a semi-diurnal tide will affect the current flow direction and flow rate in the seawater.

In our study area, the lower bound of the seawater thermocline is generally at 600 m deep and can be as deep as 800 m deep. Therefore, most of the seawater shallower than 600 m contains a fairly thick suspension layer. In consequence, most of the gas plumes in our study area can only be imaged clearly at the water depth deeper than 600 m. However, as imaged by the EK60, several gas plumes have a tilted tendency that could be associated with the bottom current (Figs. 4 to 16). In order to understand the gas plume tilt phenomenon, we compare the gas plume images with the tidal data. For that, we adopt the global ocean tide model NAO.99b (Matsumoto et al. 2000) and relate each gas plume image to the tidal variation at the same period of data acquisition. In Figs. 4 to 16, we use blue, red, yellow and green colors to mark the rising tide, ebb tide, high tide and low tide respectively.

As shown in Table 1, we have integrated the tilt directions of the EK60 plume images in Figs. 4 to 16 and different tidal conditions. Because EK60 is a single-beam detection system, the change of a gas plume image can only be observed along the ship track. Therefore, only the tilted gas plume images along the plane of the ship tracks (i.e., NE-SW orientation) are considered in this study. For that, the 201 plume images in Figs. 4 to 16 were collected when the ship's course was parallel to or against the current directions.

As shown in Fig. 11, the gas plume images from h21 to h33 in the middle portion of the southernmost Okinawa Trough indicate that the plume images incline to the northeast when the tides are rising or at high tides. At ebb tides

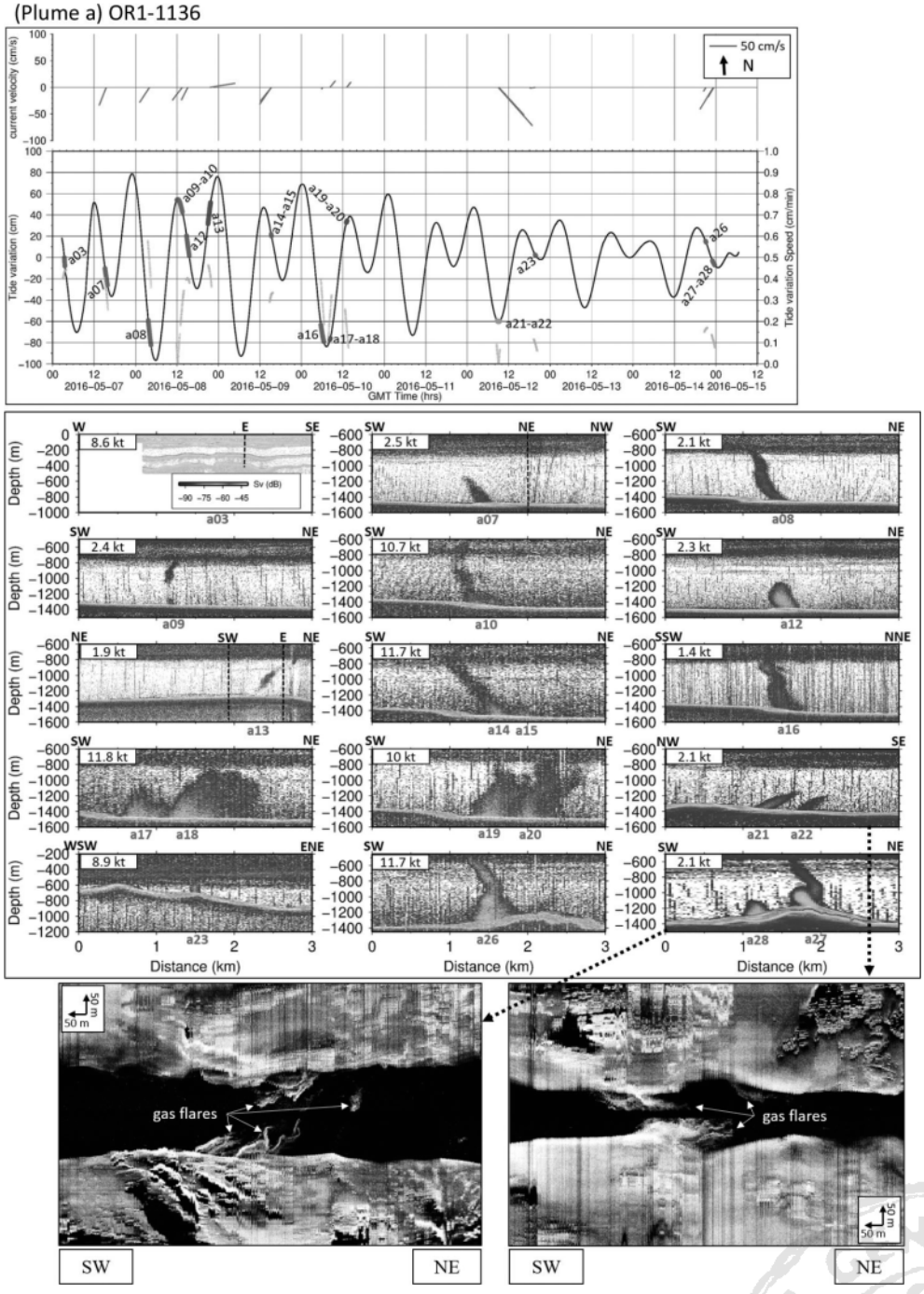


Fig. 4. EK60 images of the gas plumes of a-series. Each gas plume image is generally situated at the middle of each panel. The relatively tidal height of each plume is shown in the top panel. Four kinds of tidal situations are shown in different colors of blue, red, yellow, and green, which correspond to rising tide, ebb tide, high tide, and low tide, respectively. It is noted the plumes a21, a22, a27, and a28 have clear images in the water columns of deep-tow sidescan sonar data.

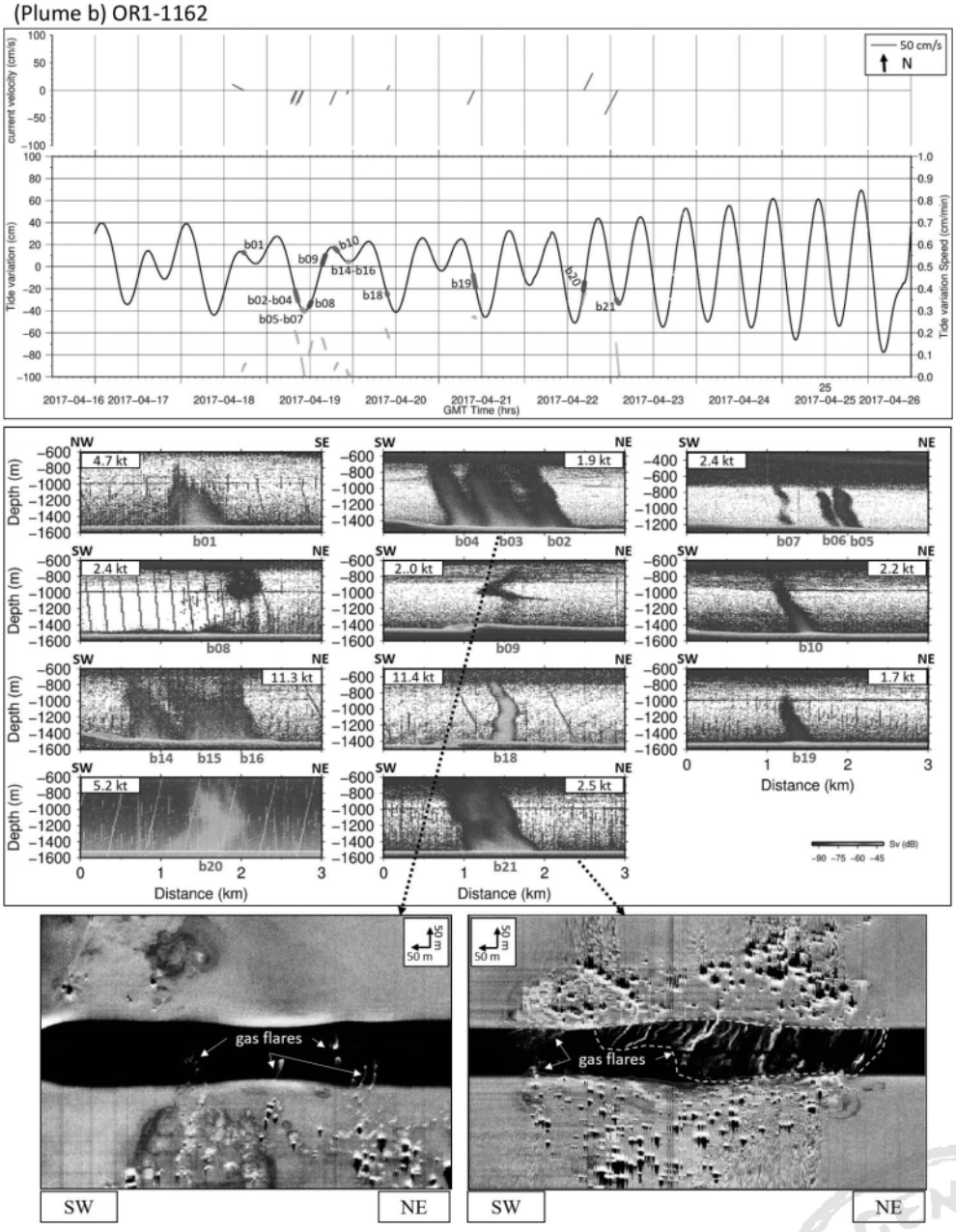


Fig. 5. EK60 images of the gas plumes of b-series. The relevant descriptions are shown in Fig. 4. The plumes b02 to b04 and b21 plumes have clear images in the water columns of deep-tow sidescan sonar data.

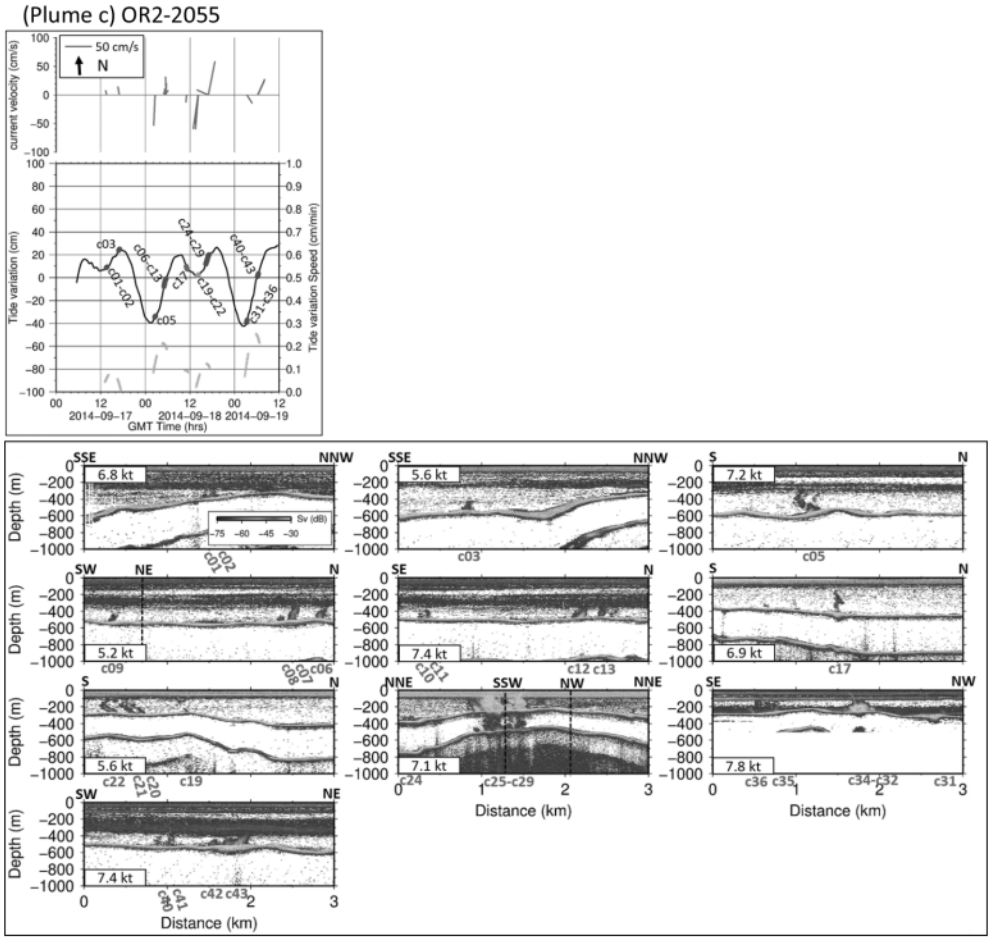


Fig. 6. EK60 images of the gas plumes of c-series. The relevant descriptions are shown in Fig. 4.

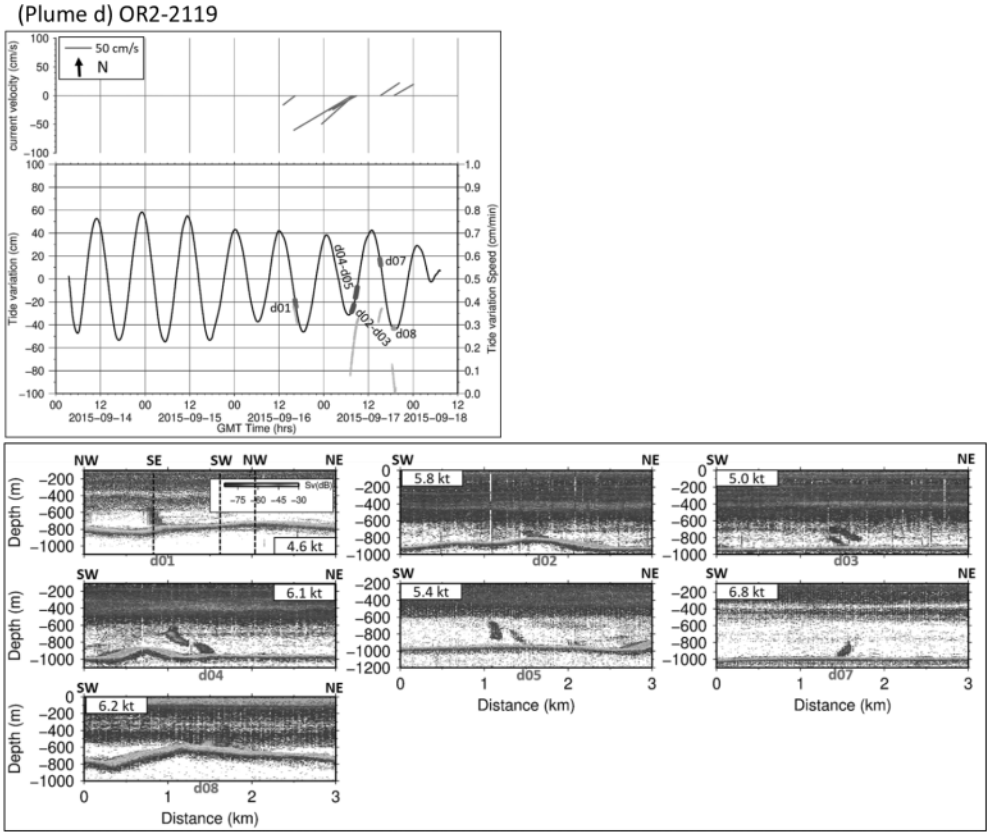


Fig. 7. EK60 images of the gas plumes of d-series. The relevant descriptions are shown in Fig. 4.

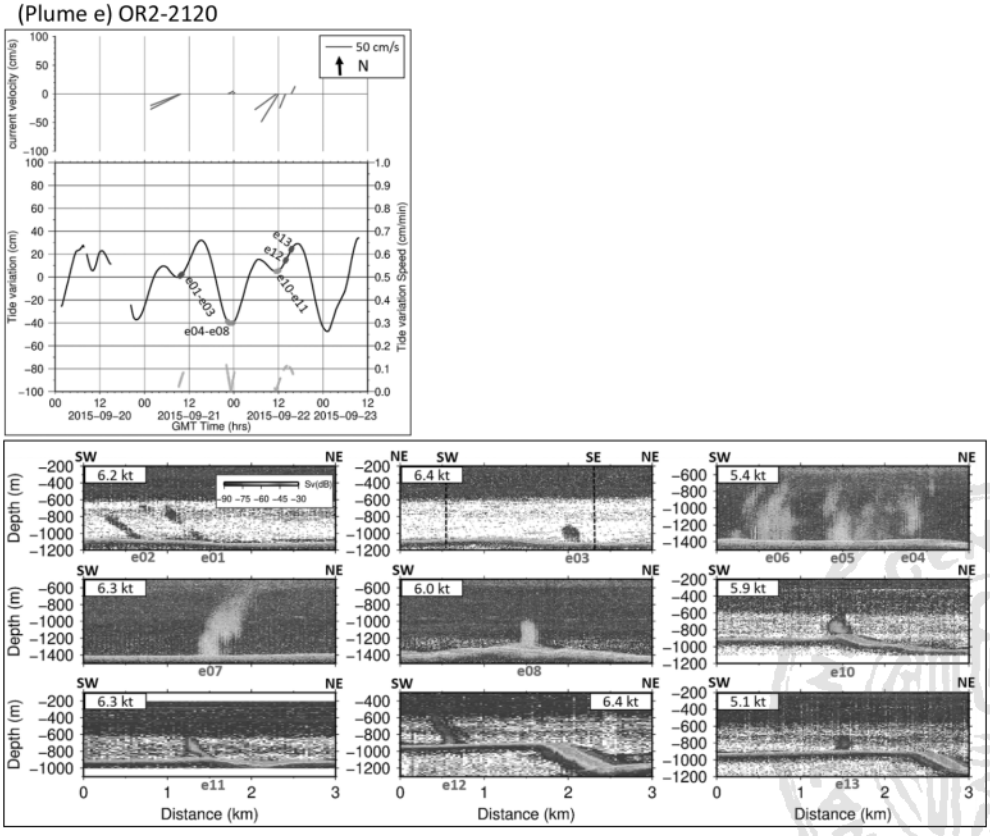


Fig. 8. EK60 images of the gas plumes of e-series. The relevant descriptions are shown in Fig. 4.

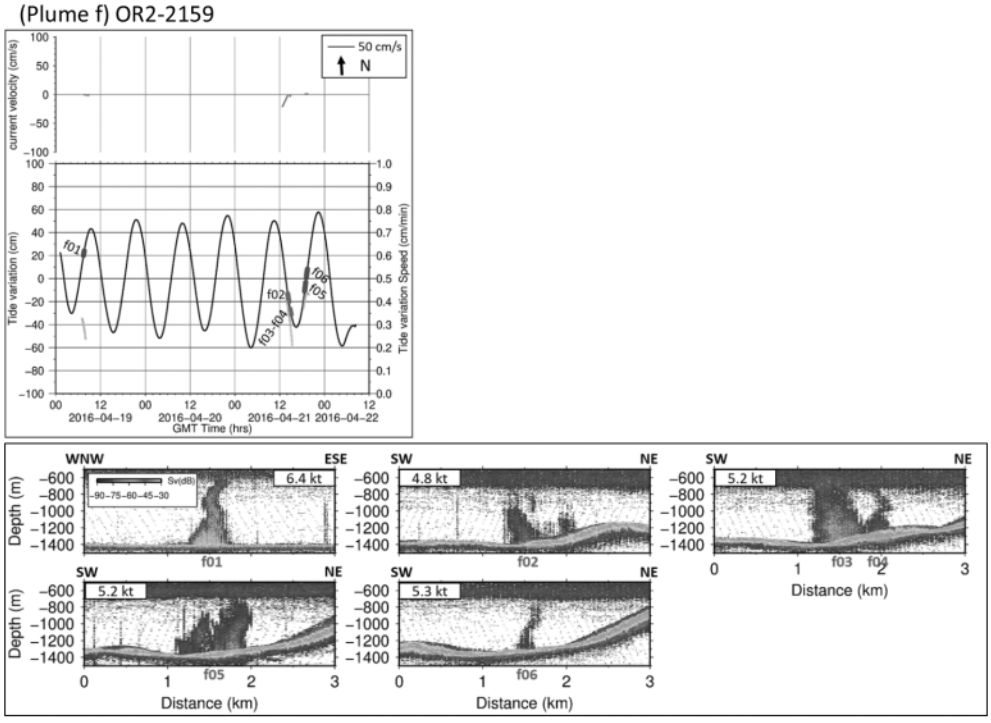


Fig. 9. EK60 images of the gas plumes of f-series. The relevant descriptions are shown in Fig. 4.

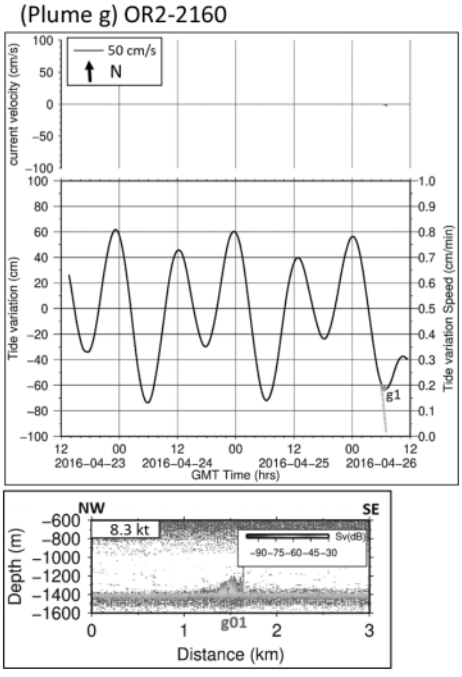


Fig. 10. EK60 image of the g01 gas plume. The relevant descriptions are shown in Fig. 4.

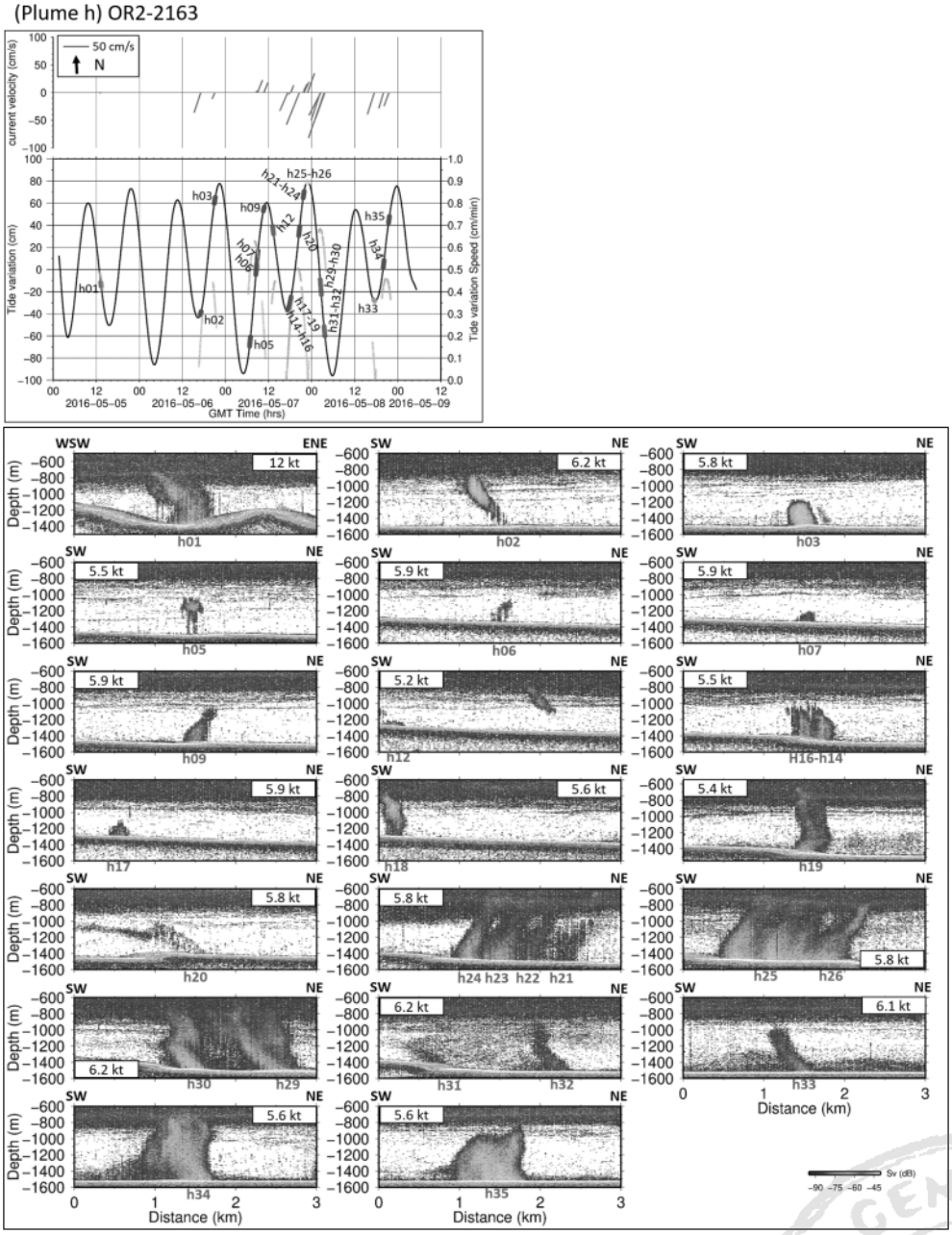


Fig. 11. EK60 images of the gas plumes of h-series. The relevant descriptions are shown in Fig. 4.

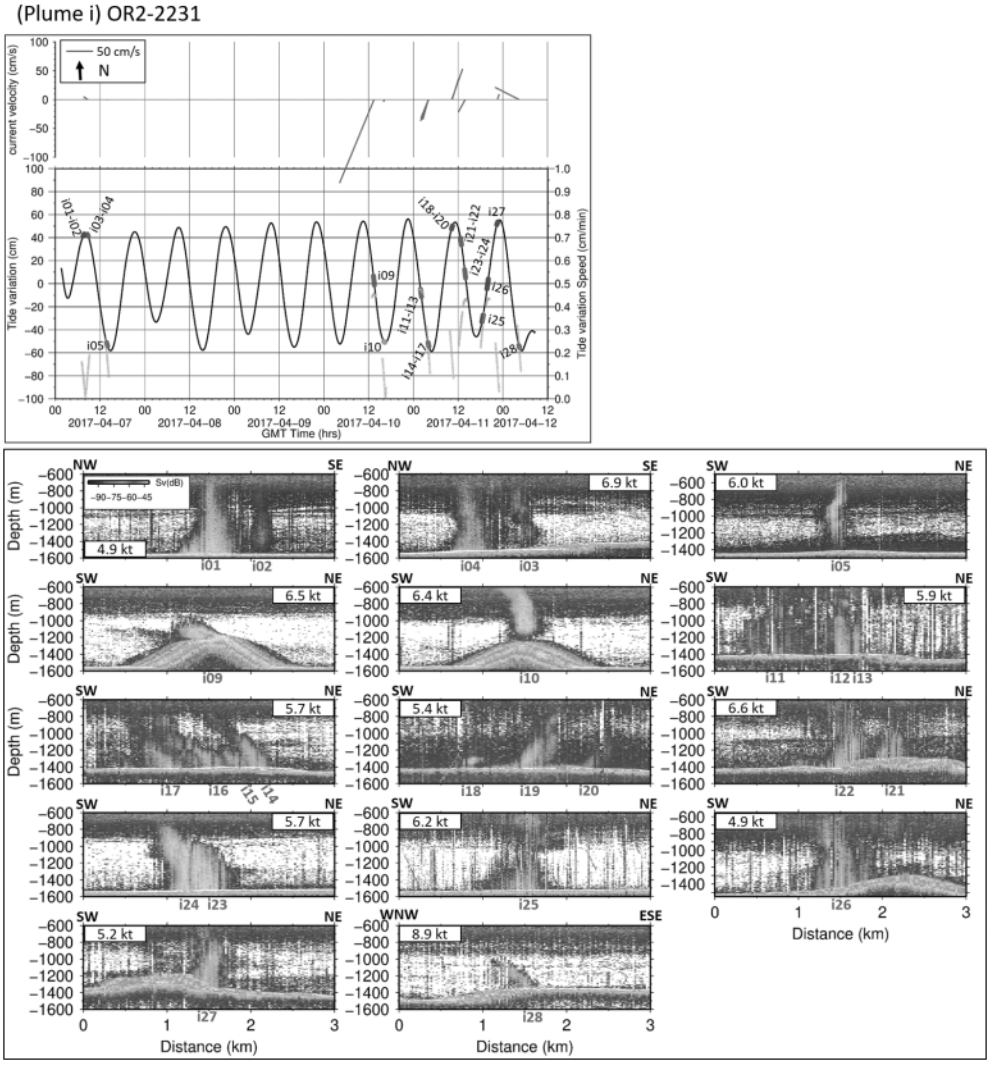


Fig. 12. EK60 images of the gas plumes of i-series. The relevant descriptions are shown in Fig. 4.

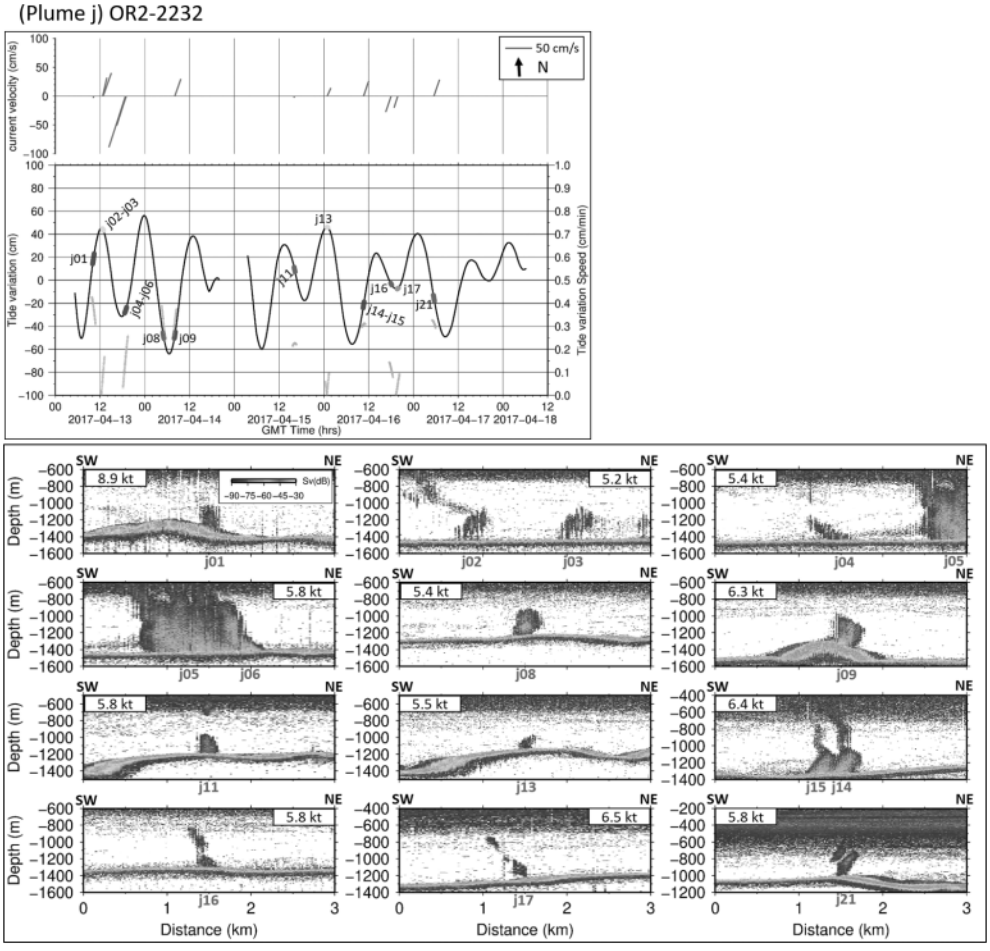


Fig. 13. EK60 images of the gas plumes of j-series. The relevant descriptions are shown in Fig. 4.

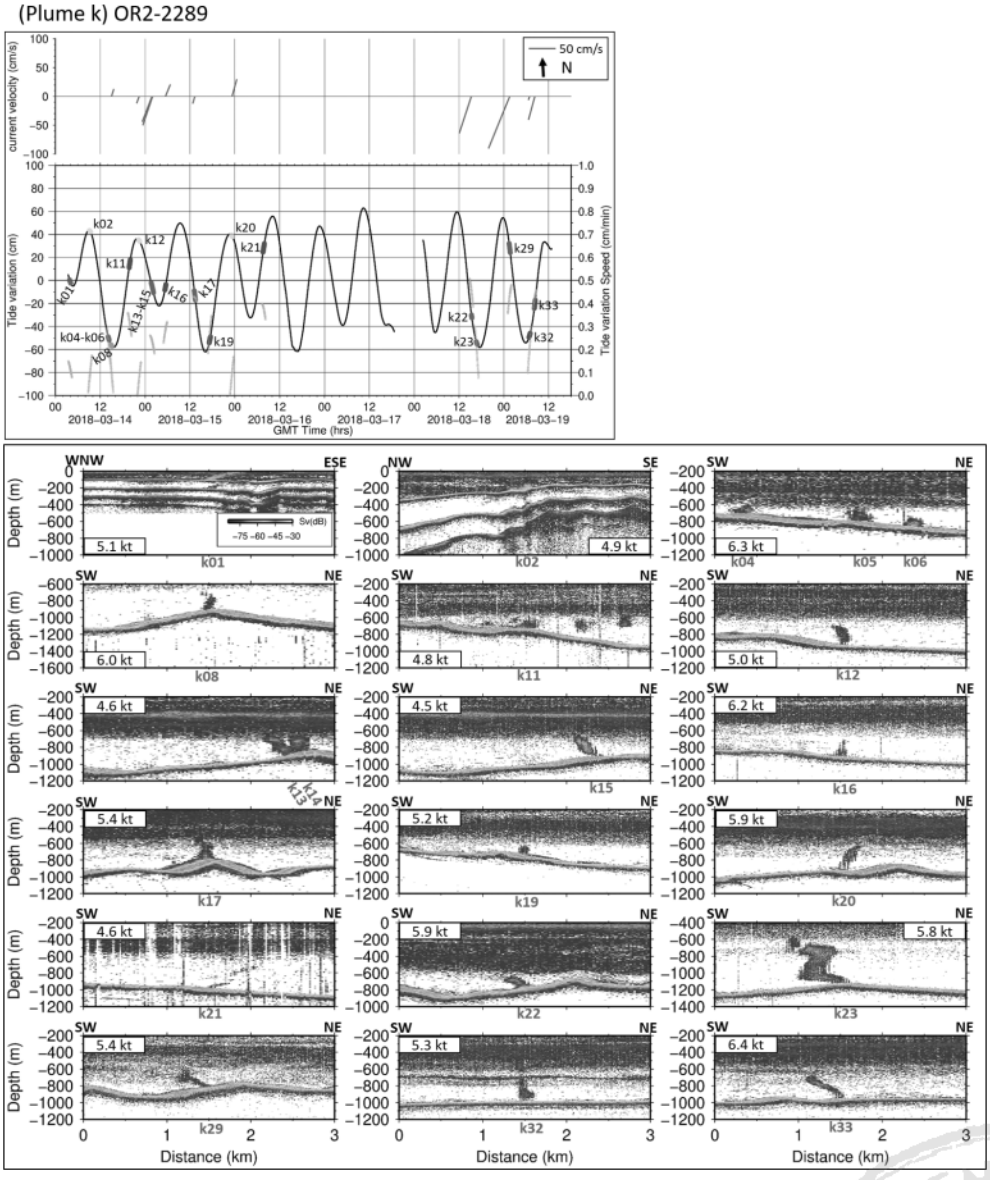


Fig. 14. EK60 images of the gas plumes of k-series. The relevant descriptions are shown in Fig. 4.

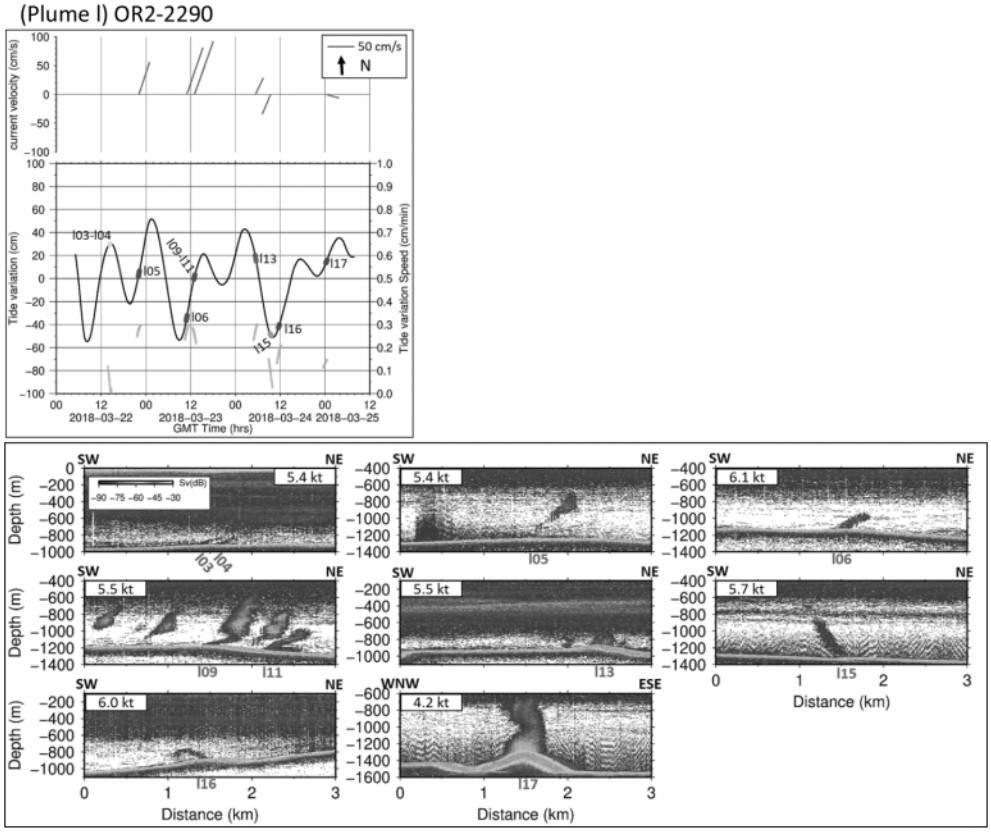


Fig. 15. EK60 images of the gas plumes of l-series. The relevant descriptions are shown in Fig. 4.

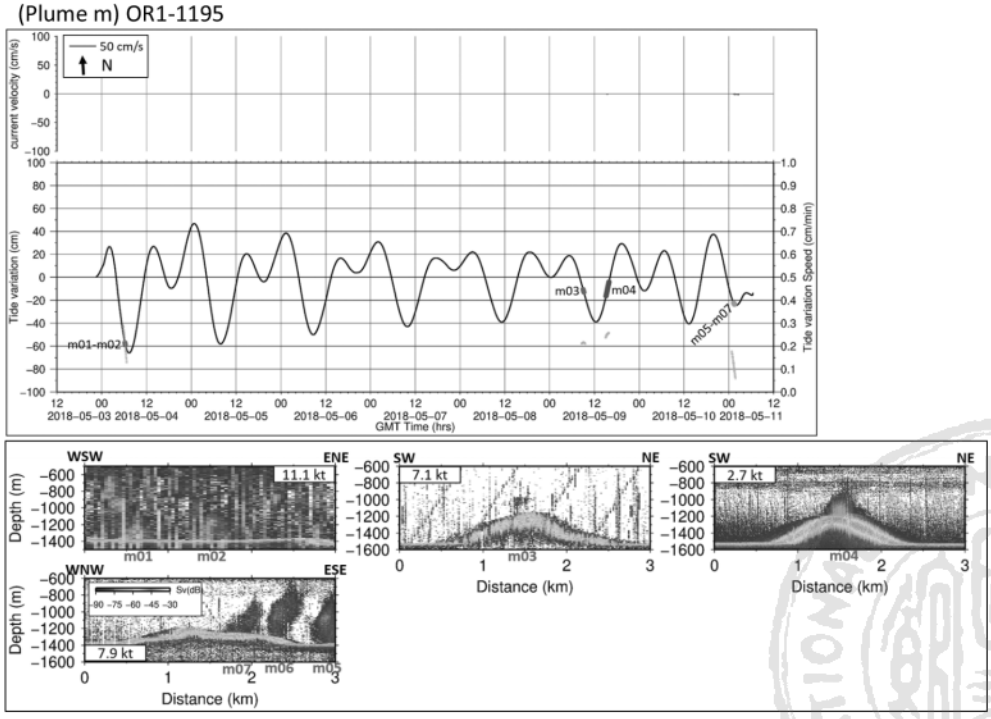


Fig. 16. EK60 images of the gas plumes of m-series. The relevant descriptions are shown in Fig. 4.

Table 1. List of gas plume tilt directions related to tidal changes in this study.

| Cruise number | Plume number (figure number) | Ship-track direction | | | | | | | | | |
|---|---|---|---|---|---|---|---|---|---|---|---|
| | | NE-SW | | NW-SE | | WNW-ESE | | ENE-WSW | | Others (NNW-SSE; N-S; NNE-SSW) | |
| OR1-1136 | a (Fig. 4) | ebb | SW | low | SE | | | | | | |
| | | rising | NE | | | | | | | | |
| OR1-1162 | b (Fig. 5) | ebb | SW | ebb | NW | | | | | | |
| | | low | SW | | | | | | | | |
| | | rising | NW | | | | | | | | |
| OR2-2055 | c (Fig. 6) | rising | NE | rising | unclear | | | | | ebb | unclear |
| | | | | | | | | | | low | S |
| | | | | | | | | | | rising | NNW |
| | | | | | | | | | | rising | N |
| | | | | | | | | | | rising | NNE |
| OR2-2119 | d (Fig. 7) | ebb | NE | low | NW | | | | | | |
| | | low | NE | | | | | | | | |
| | | rising | SW | | | | | | | | |
| OR2-2120 | e (Fig. 8) | low | NE | | | | | | | | |
| | | low | SW | | | | | | | | |
| | | rising | SW | | | | | | | | |
| OR2-2159 | f (Fig. 9) | ebb | SW | | | rising | ESE | | | | |
| | | rising | NE | | | | | | | | |
| OR2-2160 | g (Fig. 10) | | | low | unclear | | | | | | |
| OR2-2163 | h (Fig. 11) | ebb | SW | ebb | unclear | | | ebb | WSW | | |
| | | low | SW | | | | | | | | |
| | | rising | NE | | | | | | | | |
| | | high | NE | | | | | | | | |
| OR2-2231 | i (Fig. 12) | ebb | SW | ebb | unclear | ebb | WNW | | | | |
| | | rising | NE | rising | unclear | | | | | | |
| OR2-2232 | j (Fig. 13) | low | SW | | | | | | | | |
| | | rising | NE | | | | | | | | |
| | | high | NE | | | | | | | | |
| | | ebb | NE | | | | | | | | |
| | | rising | SW | | | | | | | | |
| OR2-2289 | k (Fig. 14) | ebb | SW | | | ebb | ESE | | | | |
| | | rising | NE | | | | | | | | |
| | | high | NE | | | | | | | | |
| | | ebb | NE | | | | | | | | |
| | | low | NE | | | | | | | | |
| | | rising | SW | | | | | | | | |
| OR2-2290 | l (Fig. 15) | low | SW | | | | | | | | |
| | | rising | NE | | | | | | | | |
| | | high | NE | | | | | | | | |
| | | ebb | NE | | | | | | | | |
| OR1-1195 | m (Fig. 16) | ebb | unclear | | | low | ESE | ebb | unclear | | |
| | | rising | unclear | | | | | | | | |

or at the lowest tides, the plume images incline to the southwest. As shown in d02 to d08 in Fig. 7, the plume images in the Keelung continental slope area incline to the southwest when the tide is rising. The plume images incline to the northeast when the tides are on the ebb. At the lowest tide, the plumes keep the same direction as on the ebb. However, in the areas around the Meinhua Canyon, there is no consistent tilt of the gas plumes (Fig. 13).

Furushima and Yamamoto (2015) have used ADCP to observe bottom currents in the Hatoma Knoll hydrothermal circulation area of the southern Okinawa Trough in April 2004 and May 2005. Their results showed that the bottom currents have a variation of 12-h semi-diurnal tidal cycle. During the rising tide, the water current flows northward; conversely, during the ebb tide, the water current flows southward. Their result is consistent with the results that we have observed the plume images in the central portion of the southwestern Okinawa Trough. Similarly, our deep-tow side-scan sonar images in Figs. 5 and 17 also indicate that the hydrothermal fluid from a single black chimney flows southward. Because the gas plumes keep the same direction at the rising tide to the highest tide and the same direction is on the ebb and at lowest tide, there could be a time lag effect of the tidal rise and fall effect on the flow of the water layer. It agrees with a stable flow of ~3 h during the transition of the rising and ebb (Furushima and Yamamoto 2015).

### 3.3 Near-Bottom Current Velocities Estimated from Gas Plume Images

As mentioned previously, the bottom currents as well as gas plume images can be affected by tidal variation. A real observation of the bottom current speeds will be implemented soon by ocean-bottom current meters by Academic Sinica. However, in the case of lacking real ADCP observations near seafloor, the tilted images of gas plumes from seabed could provide an alternative way to estimate near-seafloor current velocities. As illustrated in Fig. 18, a gas plume image is related to a bottom current velocity. We can measure each plume height h from the seafloor to the top of a plume, and the horizontal distance d. The rising time $\Delta t$ of a gas bubble from the seafloor to the top of the plume could be calculated by h/Vp, where Vp is the upward velocity of the gas bubbles of the plume. Then, the near seafloor current velocity Vc can be calculated by $d/\Delta t$. In that case, the value Vp is a critical for calculating the current velocity Vc. Because the bottom-current velocity (Vc) is a linear function of upward velocity of the bubbles (Vp). The error estimation of the Vc is thus proportional to the error estimation of Vp.

Xu et al. (2013) have observed Vp of the hydrothermal plume of the Main Endeavour Field in the Juan de Fuca Ridge area by using the Cabled Observatory Vent Imaging Sonar (COVIS) instrument. They found the Vp of the hydrothermal plume is between 0.11 and 0.24 m $s^{-1}$. Using the temperature anomaly observed by CTD, Cen et al. (2017) have established a dynamic mode of the hydrothermal plume in the middle Okinawa Trough and obtained a Vp of 0.35 m $s^{-1}$. In the southern Okinawa Trough, Chi (2017) used ROV images of Wang (2016) and obtained a bubble rising velocity of 0.47 m $s^{-1}$ in YK4-1 (Yonaguni Knoll IV-1) and 0.32 m $s^{-1}$ in PFZ (Penglai Fault Zone) (Figs. 2 and 3).

Veloso et al. (2015) showed that clean or dirty bubbles have slightly different rising velocities. However, the bubbles in the middle or southern Okinawa Trough have faster rising velocities (Cen et al. 2017; Chi 2017). The reason could be ascribed to a very active backarc basin rifting and an active hydrothermal circulation in the Okinawa Trough. Here, we use the Vp value of 0.47 m $s^{-1}$ from Chi (2017) to estimate the maximum near seafloor current velocities (Vc) in our study area. The results are shown in Table 2 and Figs. 4 to 16.

Belonged to 6 hydrothermal circulation zones, 11 plume images are used for further analysis (Table 1, Figs. 2, 4, 5, 11, and 13). Except for FDV-2 (Fire Dragon Volcano 2), the rest of the plumes are located near the rifting center of the Okinawa Trough (Figs. 2 and 3). Those plume images are detected along the survey tracks in the NE-SW orientation. The estimated current velocities are based on the rising speed of bubble at 0.47 m $s^{-1}$ (Table 2). In the 6 hydrothermal circulation zones, the tides flow to the NE during the rising tide and the highest tide, and flow to the SW during the ebb tide and the lowest tide (Table 1). The gas plumes are situated in the water depths from 1150 to 1550 m (Table 2); in other words, the 7° beam width of EK60 indicates that the coverage of a single footprint is between 140 and 190 m in diameter. Hence, each of our estimated current velocities can be considered as an average of the near-seafloor current velocities from the bottom to the top of the gas plume. All the estimated near-seafloor current velocities are shown in Table 2.

Our estimated near-seafloor current velocities show the slowest velocity of 2.5 cm $s^{-1}$ occurs in region YK4-1 and the fastest velocity of 156.9 cm $s^{-1}$ occurs in region FDV-1 (Fire Dragon Volcano 1). As mentioned previously, tidal variations can affect gas plume directions and the directions of the currents. In order to understand the relationship between current velocities and the tidal variations, we calculated the slope change of the tides between 15 min before and after the plume recorded time (Table 2; Figs. 4 to 16). The results show that the slopes of the tides do not influence much the near-seafloor current velocities in region YK4-1. Nevertheless, the gas plumes i09 and i10 in submarine volcano region FDV-1 do display different tilt angles of plumes (Fig. 12), demonstrating the tidal variation influence. One possible reason is that the upward velocities of the bubbles (plumes) are different at two different times because the different emissions of the gases out of the seabed at different water pressures

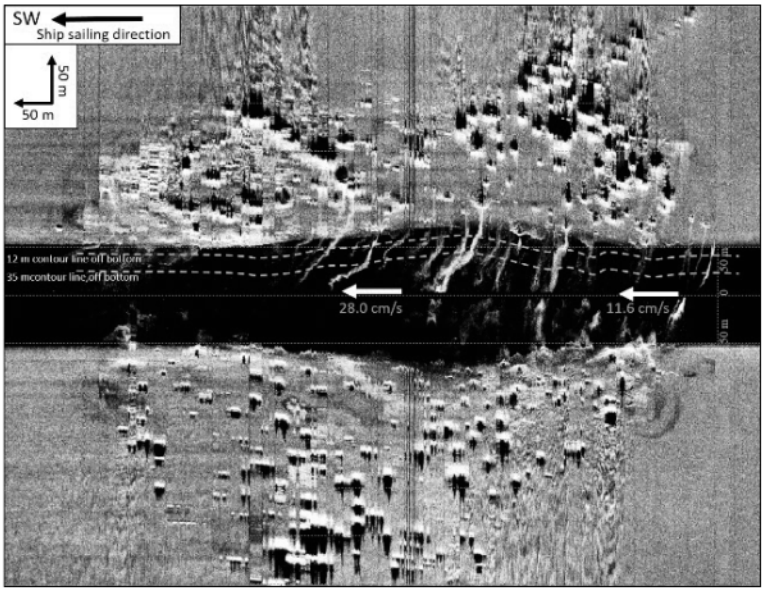


Fig. 17. Estimated near-seafloor current velocities in the deep-tow sidescan sonar image (Hsu 2017), collected simultaneously with plume image b21 in Fig. 5.

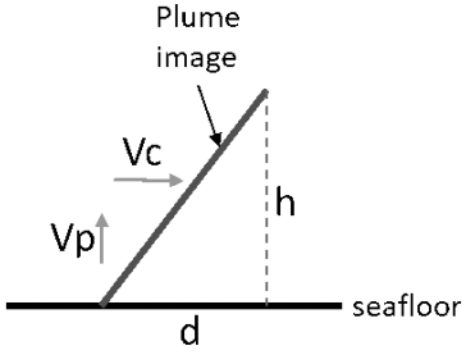


Fig. 18. Schematic relationship between current velocity Vc and upward gas bubbles (plume) float speed Vp. h is the height of the plume from the seabed; d is the horizontal distance of the plume tilt.

Table 2. Estimated near-seafloor current velocities (Vc) from 11 gas plumes.

| Plume number (figure number) | distribution area | Water depth (m) | Plume height (m) | current velocity (cm $s^{-1}$) | 30-minute tidal slopes before and after the plume (cm $min^{-1}$) |
|---|---|---|---|---|---|
| a08 (Fig. 4) | PFZ | -1447 | 628 | 34.0 | 0.579 - 0.359 |
| b04 (Fig. 5) | PFZ | -1471 | 758 | 23.7 | 0.209 - 0.153 |
| b10 (Fig. 5) | PFZ | -1503 | 573 | 28.6 | 0.032 - 0.064 |
| h24 (Fig. 11) | PFZ | -1465 | 831 | 21.2 | 0.420 - 0.217 |
| b19 (Fig. 5) | GLM | -1516 | 632 | 28.1 | 0.269 - 0.264 |
| b21 (Fig. 5) | GLM | -1516 | 949 | 49.0 | 0.154 - 0.012 |
| f05 (Fig. 9) | YK4-1 | -1333 | 610 | 2.5 | 0.371 - 0.437 |
| j09 (Fig. 13) | FDV-2 | -1390 | 388 | 31.4 | 0.238 - 0.375 |
| i14 (Fig. 12) | MHV | -1380 | 605 | 36.2 | 0.314 - 0.110 |
| i19 (Fig. 12) | MHV | -1381 | 651 | 33.1 | 0.293 - 0.088 |
| i09 (Fig. 12) | FDV-1 | -1187 | 220 | 156.9 | 0.440 - 0.443 |

(depending on the tidal variation). The different inclusions of gases into the seawater can largely change the densities of the plumes and thus the buoyancies of the plumes.

As shown in Table 2, the near-seafloor currents show different velocities. However, it is remarkable that there is a large variation of estimated current velocities in the submarine volcanic area (in areas YK4-1, FDV-1, FDV-2, and MHV in Table 2). Tectonically, submarine volcanic areas contain more volcanic gases in the sediments, thus variable gas emissions and the upward velocities of the plumes appear in submarine volcanic areas. On the contrary, in the relatively "smooth" seafloor areas such as in regions PFZ and GLM (Geolin Mounds), the estimated current velocities are considerably consistent (Table 2). In fact, by using ADCP, Furushima and Yamamoto (2015) also observed variable current velocities at the same site; at 4 m above the seafloor, the current velocities can have a variation of 20 cm $s^{-1}$, and at 62 m above the seafloor the current velocities can have a variation of 50 cm $s^{-1}$ (Furushima and Yamamoto 2015). Their observation is consistent with our values in plume b21 estimated from the deep-tow side-scan sonar (Fig. 4); the near-seafloor current velocity Vc has increased from 11.6 to 28.0 cm $s^{-1}$.

## 4. CONCLUSION

After analyzing the single-beam EK60 echo sounder data in the seawater and comparing the gas plume images with tides in the southernmost Okinawa Trough, we can draw the following conclusions.

(1) In total, 266 active gas plumes out of seabed are found. Most of the plumes are related to submarine volcanoes or hydrothermal circulation.

(2) In the middle of the southernmost Okinawa Trough, the lower boundary of thermocline generally appears around 600 m deep; therefore, most of the areas shallower than 600 m deep have a fairly thick suspension layer.

(3) The tilts of the gas plumes are changeable; they depend on the semi-diurnal tidal variation.

(4) In the middle of the southernmost Okinawa trough, the gas plumes incline to the northeast during the rising tide and highest tide, indicating that the near-seafloor current flows northeastward during that period. In contrast, the gas plumes incline to the southwest on the ebb tide and at low tide, indicating that the near-seafloor current flows southwestward during that period (Fig. 19).

(5) In the Keelung continental slope area, the gas plume images incline to the southwest at rising tide and highest tide, indicating a southwestward flow of the near-seafloor current. At ebb tide and low tide, the gas plume images incline to the northeast, indicating a northeastward flow of the near-seafloor current. This result is in opposite to the flows in the middle of the southernmost Okinawa Trough (Fig. 19).

(6) Our estimated velocities of the near-seafloor currents in the submarine volcanic area range between 2 and

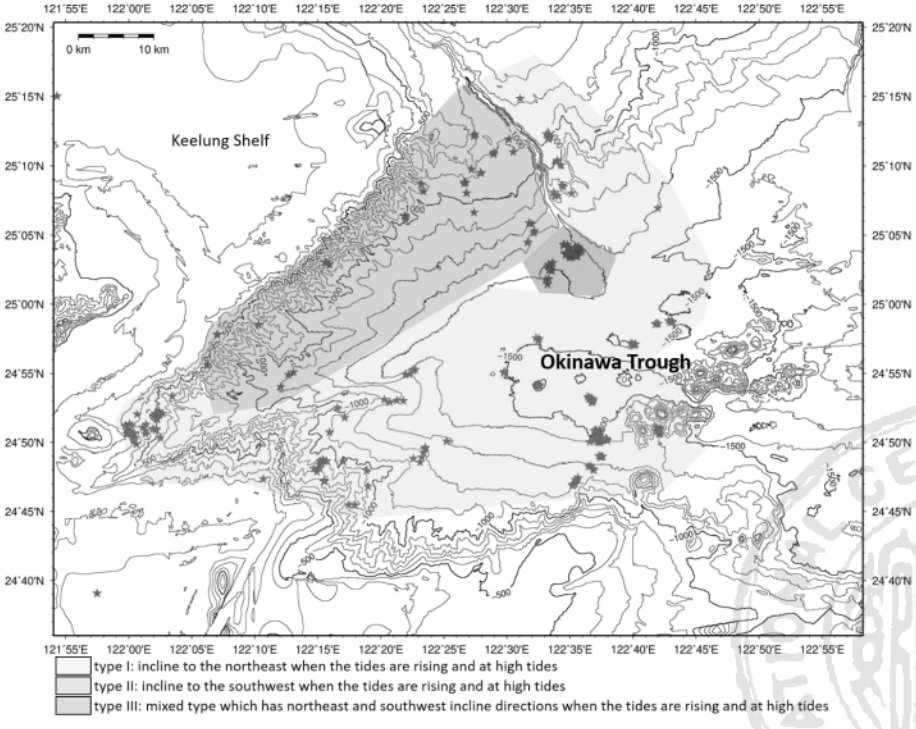


Fig. 19. The distribution of the gas plumes (red starts) and near-seafloor current patterns in the southernmost Okinawa Trough derived from acoustic echo sounders.

160 cm $s^{-1}$. However, in the relatively flat area, the near-seafloor currents are relatively stable with velocities between 20 and 50 cm $s^{-1}$. The rising bubbles (and plume) velocity used in the bottom current velocity estimation can be different and related to the quantity of the volcanic gas at each plume site, as gases in sediments are very compressible during a tidal variation.

(7) The near-seafloor bottom currents could be significantly estimated from EK plume images in the case of lacking real observations of bottom currents.

**Acknowledgements** This study was supported by the Ministry of Science and Technology (MOST) and the Central Geological Survey (CGS), Ministry of Economic Affairs, Taiwan. We appreciate the crew of R/V Ocean Researcher I and II for helping the collection of data.

## REFERENCES

Aucan, J., M. A. Merrifield, D. S. Luther, and P. Flament, 2006: Tidal mixing events on the deep flanks of Kaena ridge, Hawaii. *J. Phys. Oceanogr.*, **36**, 1202-1219, doi: 10.1175/jpo2888.1. [Link]

Baker, E. T., C. R. German, and H. Elderfield, 1995: Hydrothermal plumes over spreading-center axes: Global distributions and geological inferences. In: Humphris, S. E., R. A. Zierenberg, L. S. Mullineaux, and R. E. Thomson (Eds.), Seafloor Hydrothermal Systems: Physical, Chemical, Biological, and Geological Interactions, Volume 91, American Geophysical Union, 47-71, doi: 10.1029/GM091p0047. [Link]

Berdeal, I. G., 2006: Hydrography and flow in the axial valley of the Endeavour segment: Implications for larval dispersal. Ph.D. Thesis, University of Washington, Washington, D. C.

Cen, X.-R., S.-X. Guo, Y.-Z. Lu, Q.-U. Ling, and S.-Q. Zhou, 2017: Numerical simulation of the dynamical processes of hydrothermal plumes in Okinawa trough. *Oceanologia et Limnologia Sinica*, **48**, 1435-1445, doi: 10.11693/hyhz20170500148. (in Chinese) [Link]

Chen, S.-C., S.-K. Hsu, C.-H. Tsai, C.-Y. Ku, Y.-C. Yeh, and Y. Wang, 2010: Gas seepage, pockmarks and mud volcanoes in the near shore of SW Taiwan. *Mar. Geophys. Res.*, **31**, 133-147, doi: 10.1007/s11001-010-9097-6. [Link]

Chi, W.-C., 2017: Geological Investigation of Mineral Resource Potential in the Offshore Northeastern Taiwan: Fluid migration modeling in the mineral resource potential area (2/4). Report of Central Geological Survey, 106-12-C, 45 pp. (in Chinese with English abstract)

Crone, T. J., W. S. D. Wilcock, and R. E. McDuff, 2010: Flow rate perturbations in a black smoker hydrothermal vent in response to a mid-ocean ridge earthquake swarm. *Geochem. Geophys. Geosyst.*, **11**, Q03012, doi: 10.1029/2009GC002926. [Link]

Fujioka, K. and K. Mitsuzawa, 2001: Tide-related variability of hydrothermal activity at the TAG hydrothermal mound, mid-Atlantic Ridge and the East Pacific Rise. *J. Geodetic Soc. Jap.*, **47**, 434-440, doi: 10.11366/sokuchi1954.47.434. [Link]

Fujioka, K., K. Kobayashi, K. Kato, M. Aoki, K. Mitsuzawa, M. Kinoshita, and A. Nishizawa, 1997: Tide-related variability of TAG hydrothermal activity observed by deep-sea monitoring system and OBSH. *Earth Planet. Sci. Lett.*, **153**, 239-250, doi: 10.1016/s0012-821x(97)00174-x. [Link]

Furushima, Y. and H. Yamamoto, 2015: Periodic Behavior of Deep Sea Current in the Hatoma Knoll Hydrothermal System. In: Ishibashi J., K. Okino, and M. Sunamura (Eds.), Subseafloor Biosphere Linked to Hydrothermal Systems, Springer, Tokyo, 625-637, doi: 10.1007/978-4-431-54865-2_50. [Link]

German, C. R., J. Briem, C. Chin, M. Danielsen, S. Holland, R. James, A. Jónsdóttir, E. Ludford, C. Moser, J. Ólafsson, M. R. Palmer, and M. D. Rudnicki, 1994: Hydrothermal activity on the Reykjanes Ridge: the Steinahóll vent-field at 63°06'N. *Earth Planet. Sci. Lett.*, **121**, 647-654, doi: 10.1016/0012-821x(94)90098-1. [Link]

Heeschen, K. U., A. M. Tréhu, R. W. Collier, E. Suess, and G. Rehder, 2003: Distribution and height of methane bubble plumes on the Cascadia Margin characterized by acoustic imaging. *Geophys. Res. Lett.*, **30**, doi: 10.1029/2003gl016974. [Link]

Hsu, S.-K., 2017: Geological Investigation of Mineral Resource Potential in the Offshore Northeastern Taiwan: High-resolution Sonar and Magnetic Surveys (2/4). Report of Central Geological Survey, 106-13, 237 pp. (in Chinese with English abstract)

Hsu, S.-K., J.-C. Sibuet, S. Monti, C.-T. Shyu, and C.-S. Liu, 1996: Transition between the Okinawa trough backarc extension and the Taiwan collision: New insights on the southernmost Ryukyu subduction zone. *Mar. Geophys. Res.*, **18**, 163-187, doi: 10.1007/bf00286076. [Link]

Hsu, S.-K., S.-S. Lin, S.-Y. Wang, C.-H. Tsai, W.-B. Doo, S.-C. Chen, J.-Y. Lin, Y.-C. Yeh, H.-F. Wang, and C.-W. Su, 2018: Seabed gas emissions and submarine landslides off SW Taiwan. *Terr. Atmos. Ocean. Sci.*, **29**, 7-15, doi: 10.3319/TAO.2016.10.04.01. [Link]

Kimura, M., 1985: Back-arc rifting in the Okinawa Trough. *Mar. Petrol. Geol.*, **2**, 222-240, doi: 10.1016/0264-8172(85)90012-1. [Link]

Kimura, M., I. Kaneoka, Y. Kato, S. Yamamoto, I. Kushiro, H. Tokuyama, H. Kinoshita, N. Isezaki, H. Masaki, A. Oshida, S. Uyeda, and T. W. C. Hilde, 1986: Report on DELP 1984 cruises in the middle Okinawa Trough Part V: Topography and geology of the central grabens and their vicinity. *Bulletin of the Earthquake Research Institute of Tokyo University*, **61**, 269-310.

Kimura, M., S. Uyeda, Y. Kato, T. Tanaka, M. Yamano, T. Gamo, H. Sakai, S. Kato, E. Izawa, and T. Oomori, 1988: Active hydrothermal mounds in the Okinawa Trough backarc basin, Japan. *Tectonophysics*, **145**, 319-324, doi: 10.1016/0040-1951(88)90203-x. [Link]

Lallemand, S. E., C.-S. Liu, and the ACT cruise scientific team, 1997: Swath bathymetry reveals active arc-continent collision near Taiwan. *Eos, Trans. AGU*, **78**, 173-175, doi: 10.1029/97eo00116. [Link]

Larson, B. I., E. J. Olson, and M. D. Lilley, 2007: In situ measurement of dissolved chloride in high temperature hydrothermal fluids. *Geochim. Cosmochim. Acta*, **71**, 2510-2523, doi: 10.1016/j.gca.2007.02.013. [Link]

Lee, C.-S., G.-G. Shor, L. D. Bibee, R.-S. Lu, and T. W. Hilde, 1980: Okinawa Trough: Origin of a back-arc basin. *Mar. Geol.*, **35**, 219-241, doi: 10.1016/0025-3227(80)90032-8. [Link]

Lee, Y.-L., 2005: The study of active submarine volcanoes and hydrothermal vents in the Southernmost Part of Okinawa Trough. Master Thesis, Institute of Applied Geophysics, National Taiwan Ocean University, Keelung, Taiwan, 44 pp. (in Chinese)

Letouzey, J. and M. Kimura, 1985: Okinawa Trough genesis: Structure and evolution of a backarc basin developed in a continent. *Mar. Petrol. Geol.*, **2**, 111-130, doi: 10.1016/0264-8172(85)90002-9. [Link]

Lin, J.-Y., J.-C. Sibuet, C.-S. Lee, S.-K. Hsu, and F. Klingelhoefer, 2007: Origin of the southern Okinawa Trough volcanism from detailed seismic tomography. *J. Geophys. Res.*, **112**, B08308, doi: 10.1029/2006JB004703. [Link]

Lin, J.-Y., J.-C. Sibuet, C.-S. Lee, S.-K. Hsu, F. Klingelhoefer, Y. Auffret, P. Pelleau, J. Crozon, and C.-H. Lin, 2009: Microseismicity and faulting in the southwestern Okinawa Trough. *Tectonophysics*, **466**, 268-280, doi: 10.1016/j.tecto.2007.11.030. [Link]

Massoth, G. J., H. B. Milburn, S. R. Hammond, D. A. Butterfield, R. E. McDuff, and J. E. Lupton, 1988: The geochemistry of submarine venting fluids at Axial Volcano, Juan de Fuca Ridge: New sampling methods and a VENTS Program rationale. In: De Luca, M. P. and I. Babb (Eds.), Global Venting, Midwater, and Benthic Ecological Processes, National Undersea Research Program Report 88-4, NOAA, Rockvile, MD, 29-59.

Matsumoto, K., T. Takanezawa, and M. Ooe, 2000: Ocean Tide Models Developed by Assimilating TOPEX/POSEIDON Altimeter Data into Hydrodynamical Model: A Global Model and a Regional Model around Japan. *J. Oceanogr.*, **56**, 567-581, doi: 10.1023/A:1011157212596. [Link]

Naudts, L., J. Greinert, Y. Artemov, P. Staelens, J. Poort, P. Van Rensbergen, and M. De Batist, 2006: Geological and morphological setting of 2778 methane seeps in the Dnepr paleo-delta, northwestern Black Sea. *Mar. Geol.*, **227**, 177-199, doi: 10.1016/j.margeo.2005.10.005. [Link]

Polikarpov, G. G., V. N. Egorov, A. I. Nezhdanonv, S. B. Gulin, Y. D. Kulev, and M. B. Gulin, 1989: Methane gas seeps in the Black Sea: A new object of molismology. In: Polikarpov, G. G. (Ed.), Molismology of the Black Sea, Kiev, Nauka, 10-20.

Seno, T., S. Stein, and A. E. Gripp, 1993: A model for the motion of the Philippine Sea Plate consistent with NUVEL-1 and geological data. *J. Geophys. Res.*, **98**, 17941-17948, doi: 10.1029/93JB00782. [Link]

Shyu, C.-T. and C.-S. Liu, 2001: Heat Flow of the Southwestern End of the Okinawa Trough. *Terr. Atmos. Ocean. Sci.*, **12**, 305-317, doi: 10.3319/TAO.2001.12.S.305(ODP). [Link]

Sibuet, J.-C., J. Letouzey, F. Barbier, J. Charvet, J.-P. Foucher, T. W. C. Hilde, M. Kimura, L.-Y. Chiao, B. Marsset, C. Muller, and J.-F. Stéphan, 1987: Back arc extension in the Okinawa Trough. *J. Geophys. Res.*, **92**, 14041-14063, doi: 10.1029/JB092iB13p14041. [Link]

Sibuet, J.-C., B. Deffontaines, S.-K. Hsu, N. Thareau, J. P. Le Formal, C.-S. Liu, and ACT party, 1998: Okinawa Trough backarc basin: Early tectonic and magmatic evolution. *J. Geophys. Res.*, **103**, 30245-30267, doi: 10.1029/98jb01823. [Link]

Tsai, C.-H., 1999: Submarine Volcanoes and Hydrothermal Circulation in the Southernmost Part of Okinawa Trough: An Initial Study. Master Thesis, Institute of Applied Geophysics, National Taiwan Ocean University, Keelung, Taiwan, 82 pp. (in Chinese)

Urban, P., K. Köser, and J. Greinert, 2017: Processing of multibeam water column image data for automated bubble/seep detection and repeated mapping. *Limnol. Oceanogr.*, **15**, 1-21, doi: 10.1002/lom3.10138. [Link]

Uyeda, S., 1977: Some basic problems in the trench-arc-back arc system. In: Talwani, M. and W. C. Pitman (Eds.), Island Arcs, Deep Sea Trenches and Back-Arc Basins, Volume 1, American Geophysical Union, Washington, DC, 1-14, doi: 10.1029/ME001p0001. [Link]

Veirs, S. R., R. E. McDuff, and F. R. Stahr, 2006: Magnitude and variance of near-bottom horizontal heat flux at the Main Endeavour hydrothermal vent field. *Geochem. Geophys. Geosyst.*, **7**, doi: 10.1029/2005gc000952. [Link]

Veloso, M., J. Greinert, J. Mienert, and M. De Batist, 2015: A new methodology for quantifying bubble flow rates in deep water using splitbeam echosounders: Examples from the Arctic offshore NW-Svalbard. *Limnol. Oceanogr.*, **13**, 267-287, doi: 10.1002/lom3.10024. [Link]

Wang, C.-C., 2016: Geological Investigation of Mineral Resource Potential in the Offshore Northeastern Taiwan: Video Surveys and Sampling of Seafloor Mineral Deposits (1/4). Report of Central Geological Survey, 105-14-B, 70 pp. (in Chinese with English abstract)

Xu, G., D. R. Jackson, K. G. Bemis, and P. A. Rona, 2013: Observations of the volume flux of a seafloor hydrothermal plume using an acoustic imaging sonar. *Geochem. Geophys. Geosyst.*, **14**, 2369-2382, doi: 10.1002/ggge.20177. [Link]

Yu, S.-B., H.-Y. Chen, and L.-C. Kuo, 1997: Velocity field of GPS stations in the Taiwan area. *Tectonophysics*, **274**, 41-59, doi: 10.1016/s0040-1951(96)00297-1. [Link]

## APPENDIX A

Table A1. The detailed information of 266 plume images in this study (remark A means complete plume image; remark B means incomplete plume image).

| No. | longitude (degree:minute) | latitude (degree:minute) | water depth (m) | observation date (dd/mm/yyyy) | observation time (hh:mm:ss) | ship speed (kts) | plume height (m) | tidal type | remark |
|---|---|---|---|---|---|---|---|---|---|
| a01 | 121:47.43576 | 25:12.56184 | -113 | 07/05/2016 | 03:26:32 | | | | B |
| a02 | 121:47.63472 | 25:12.55806 | -107 | 07/05/2016 | 03:27:33 | | | | B |
| a03 | 121:47.65872 | 25:12.55668 | -107 | 07/05/2016 | 03:27:41 | 8.6 | 47 | ebb | A |
| a04 | 121:50.74851 | 25:12.56010 | -124 | 07/05/2016 | 09:39:17 | | | | B |
| a05 | 121:47.58168 | 25:10.59646 | -54 | 07/05/2016 | 09:40:31 | | | | B |
| a06 | 121:50.98935 | 25:10.59184 | -88 | 07/05/2016 | 03:27:40 | | | | B |
| a07 | 122:41.86062 | 24:58.59666 | -1485 | 07/05/2016 | 15:32:30 | 2.5 | 340 | ebb | A |
| a08 | 122:37.91028 | 24:50.23554 | -1447 | 08/05/2016 | 04:02:26 | 2.1 | 628 | ebb | A |
| a09 | 122:37.51998 | 24:48.97314 | -1335 | 08/05/2016 | 12:20:15 | 2.4 | 553 | high tide to ebb | A |
| a10 | 122:37.29696 | 24:50.06250 | -1447 | 08/05/2016 | 13:30:13 | 10.7 | 460 | ebb | A |
| a11 | 122:43.00716 | 24:58.69914 | -1494 | 08/05/2016 | 14:24:51 | | | | B |
| a12 | 122:43.05498 | 24:58.76298 | -1478 | 08/05/2016 | 15:08:54 | 2.3 | 326 | ebb | A |
| a13 | 122:36.89502 | 24:47.97881 | -1267 | 08/05/2016 | 21:32:34 | 1.9 | 442 | rising | A |
| a14 | 122:37.01140 | 24:50.22617 | -1466 | 09/05/2016 | 15:17:59 | 11.7 | 800 | ebb | A |
| a15 | 122:37.13220 | 24:50.37137 | -1479 | 09/05/2016 | 15:18:54 | 11.7 | 142 | ebb | A |
| a16 | 122:37.28952 | 24:50.07708 | -1448 | 10/05/2016 | 06:05:48 | 1.4 | 605 | ebb | A |
| a17 | 122:36.87420 | 24:50.27052 | -1474 | 10/05/2016 | 08:17:10 | 11.8 | 432 | rising | A |
| a18 | 122:37.15296 | 24:50.57274 | -1486 | 10/05/2016 | 08:19:03 | 11.8 | 690 | rising | A |
| a19 | 122:36.95040 | 24:50.24094 | -1470 | 10/05/2016 | 13:07:56 | 10 | 670 | rising | A |
| a20 | 122:37.12314 | 24:50.45832 | -1482 | 10/05/2016 | 13:09:36 | 10 | 826 | rising | A |
| a21 | 122:41.86537 | 24:50.80725 | -1377 | 12/05/2016 | 08:59:57 | 2.1 | 250 | low tide | A |
| a22 | 122:42.04920 | 24:50.61720 | -1396 | 12/05/2016 | 09:07:40 | 2.1 | 216 | low tide | A |
| a23 | 122:15.55134 | 24:47.17074 | -743 | 12/05/2016 | 19:45:07 | 8.9 | 132 | ebb | A |
| a24 | 121:57.50070 | 24:39.05388 | -126 | 13/05/2016 | 05:55:30 | | | | B |
| a25 | 122:22.27182 | 24:54.94032 | -1309 | 13/05/2016 | 20:08:50 | | | | B |
| a26 | 122:34.71846 | 25:03.57126 | -1355 | 14/05/2016 | 21:04:10 | 11.7 | 873 | ebb | A |
| a27 | 122:34.90614 | 25:04.02223 | -1225 | 14/05/2016 | 23:13:05 | 2.1 | 590 | ebb | A |
| a28 | 122:34.68302 | 25:03.68023 | -1315 | 14/05/2016 | 23:23:10 | 2.1 | 200 | ebb | A |
| a29 | 122:33.24162 | 25:1.433700 | -1409 | 15/05/2016 | 00:25:28 | | | | B |
| a30 | 121:49.97292 | 25:13.04082 | -123 | 15/05/2016 | 05:53:49 | | | | B |
| b01 | 122:36.53412 | 24:53.182080 | -1516 | 18/04/2017 | 17:30:37 | 4.7 | 719 | ebb | A |
| b02 | 122:37.33144 | 24:50.828171 | -1486 | 19/04/2017 | 08:09:58 | 1.9 | 763 | ebb | A |
| b03 | 122:37.19129 | 24:50.546268 | -1486 | 19/04/2017 | 08:19:39 | 1.9 | 784 | ebb | A |
| b04 | 122:37.06395 | 24:50.296641 | -1471 | 19/04/2017 | 08:27:47 | 1.9 | 758 | ebb | A |
| b05 | 122:35.62902 | 24:47.426212 | -1252 | 19/04/2017 | 10:00:08 | 2.4 | 476 | low tide | A |
| b06 | 122:35.57349 | 24:47.320465 | -1234 | 19/04/2017 | 10:03:34 | 2.4 | 434 | low tide | A |
| b07 | 122:35.41258 | 24:47.026960 | -1211 | 19/04/2017 | 10:13:07 | 2.4 | 481 | low tide | A |
| b08 | 122:36.69654 | 24:52.912200 | -1515 | 19/04/2017 | 12:10:16 | 2.4 | 768 | rising | A |
| b09 | 122:40.13232 | 24:57.080820 | -1401 | 19/04/2017 | 15:55:59 | 2 | 652 | rising | A |
| b10 | 122:37.03319 | 24:50.883776 | -1503 | 19/04/2017 | 19:21:23 | 2.2 | 573 | ebb | A |
| b11 | 122:35.21622 | 24:46.935120 | -1209 | 19/04/2017 | 21:25:42 | | | | B |
| b12 | 122:35.20493 | 24:46.871271 | -1209 | 19/04/2017 | 22:24:25 | | | | B |

Table A1. (Continued)

| No. | longitude (degree:minute) | latitude (degree:minute) | water depth (m) | observation date (dd/mm/yyyy) | observation time (hh:mm:ss) | ship speed (kts) | plume height (m) | tidal type | remark |
|---|---|---|---|---|---|---|---|---|---|
| b13 | 122:35.42186 | 24:47.298994 | -1224 | 19/04/2017 | 22:26:59 | | | | B |
| b14 | 122:36.86601 | 24:50.239885 | -1472 | 19/04/2017 | 22:44:25 | 11.3 | 769 | low tide | A |
| b15 | 122:37.03230 | 24:50.573263 | -1495 | 19/04/2017 | 22:46:23 | 11.3 | 719 | low tide | A |
| b16 | 122:37.13851 | 24:50.792554 | -1491 | 19/04/2017 | 22:47:39 | 11.3 | 752 | low tide | A |
| b17 | 122:39.84594 | 24:57.167280 | -1405 | 20/04/2017 | 02:17:38 | | | | B |
| b18 | 122:39.96714 | 24:57.082560 | -1392 | 20/04/2017 | 09:35:52 | 11.4 | 752 | ebb | A |
| b19 | 122:36.78618 | 24:53.001780 | -1516 | 21/04/2017 | 09:57:05 | 1.7 | 632 | ebb | A |
| b20 | 122:36.68766 | 24:53.148600 | -1514 | 22/04/2017 | 16:35:10 | 5.2 | 911 | rising | A |
| b21 | 122:36.54606 | 24:53.174400 | -1516 | 23/04/2017 | 02:01:34 | 2.5 | 949 | ebb | A |
| b22 | 122:36.41460 | 24:53.297880 | -1516 | 25/04/2017 | 22:45:43 | | | | B |
| b23 | 121:54.31500 | 25:15.025560 | -139 | 26/04/2017 | 08:46:02 | | | | B |
| c01 | 122:7.04100 | 24:57.77640 | -399 | 17/09/2014 | 13:36:32 | 6.8 | 78 | rising | A |
| c02 | 122:7.02564 | 24:57.83544 | -384 | 17/09/2014 | 13:37:02 | 6.8 | 90 | rising | A |
| c03 | 122:6.27378 | 24:55.58400 | -531 | 17/09/2014 | 17:00:40 | 5.6 | 118 | rising | A |
| c04 | 122:3.46080 | 24:53.31174 | -612 | 18/09/2014 | 00:03:17 | | | | B |
| c05 | 122:2.68920 | 24:52.07862 | -583 | 18/09/2014 | 02:37:20 | 7.2 | 292 | rising | A |
| c06 | 122:2.42334 | 24:52.24362 | -482 | 18/09/2014 | 05:01:27 | 5.2 | 104 | rising | A |
| c07 | 122:2.42065 | 24:52.07774 | -506 | 18/09/2014 | 05:02:55 | 5.2 | 180 | rising | A |
| c08 | 122:2.41783 | 24:52.01381 | -516 | 18/09/2014 | 05:03:29 | 5.2 | 55 | rising | A |
| c09 | 122:2.19052 | 24:50.96919 | -533 | 18/09/2014 | 05:13:15 | 5.2 | 87 | rising | A |
| c10 | 122:1.93262 | 24:50.95265 | -476 | 18/09/2014 | 05:20:21 | 7.4 | 98 | rising | A |
| c11 | 122:1.95074 | 24:50.99587 | -476 | 18/09/2014 | 05:20:57 | 7.4 | 104 | rising | A |
| c12 | 122:2.09602 | 24:51.97487 | -472 | 18/09/2014 | 05:30:59 | 7.4 | 120 | rising | A |
| c13 | 122:2.09150 | 24:52.09888 | -461 | 18/09/2014 | 05:32:01 | 7.4 | 100 | rising | A |
| c14 | 122:1.33779 | 24:50.62721 | -386 | 18/09/2014 | 08:25:37 | | | | B |
| c15 | 122:1.36107 | 24:50.83574 | -424 | 18/09/2014 | 08:27:23 | | | | B |
| c16 | 122:1.38907 | 24:51.29688 | -457 | 18/09/2014 | 08:31:13 | | | | B |
| c17 | 122:1.11996 | 24:51.08898 | -430 | 18/09/2014 | 11:06:37 | 6.9 | 262 | ebb | A |
| c18 | 122:0.67374 | 24:52.02895 | -337 | 18/09/2014 | 13:58:12 | | | | B |
| c19 | 122:0.46198 | 24:50.61269 | -253 | 18/09/2014 | 14:10:14 | 5.6 | 142 | low tide | A |
| c20 | 122:0.43200 | 24:50.33287 | -291 | 18/09/2014 | 14:12:34 | 5.6 | 128 | low tide | A |
| c21 | 122:0.42266 | 24:50.25845 | -286 | 18/09/2014 | 14:13:12 | 5.6 | 170 | low tide | A |
| c22 | 122:0.40357 | 24:50.13377 | -265 | 18/09/2014 | 14:14:16 | 5.6 | 166 | low tide | A |
| c23 | 122:0.24690 | 24:51.20742 | -378 | 18/09/2014 | 14:31:58 | | | | B |
| c24 | 122:0.07374 | 24:51.34416 | -363 | 18/09/2014 | 16:52:02 | 7.1 | 66 | rising | A |
| c25 | 121:59.9886 | 24:50.81712 | -248 | 18/09/2014 | 16:56:36 | 7.1 | 174 | rising | A |
| c26 | 121:59.9654 | 24:50.69910 | -242 | 18/09/2014 | 16:57:38 | 7.1 | 201 | rising | A |
| c27 | 121:59.9569 | 24:50.66605 | -238 | 18/09/2014 | 16:57:56 | 7.1 | 150 | rising | A |
| c28 | 121:59.9012 | 24:50.59674 | -228 | 18/09/2014 | 16:59:00 | 7.1 | 124 | rising | A |
| c29 | 121:59.8626 | 24:50.59939 | -226 | 18/09/2014 | 16:59:32 | 7.1 | 213 | rising | A |
| c30 | 121:59.7106 | 24:51.16032 | -291 | 18/09/2014 | 17:06:36 | | | | B |
| c31 | 121:59.7526 | 24:51.22082 | -295 | 19/09/2014 | 03:13:46 | 7.8 | 63 | rising | A |
| c32 | 121:59.9946 | 24:50.82802 | -251 | 19/09/2014 | 03:17:05 | 7.8 | 63 | rising | A |
| c33 | 122:0.03654 | 24:50.75773 | -250 | 19/09/2014 | 03:17:41 | 7.8 | 196 | rising | A |
| c34 | 122:0.09400 | 24:50.68038 | -257 | 19/09/2014 | 03:18:23 | 7.8 | 79 | rising | A |
| c35 | 122:0.34722 | 24:50.29332 | -252 | 19/09/2014 | 03:21:45 | 7.8 | 126 | rising | A |
| c36 | 122:0.44634 | 24:50.14902 | -278 | 19/09/2014 | 03:23:01 | 7.8 | 150 | rising | A |
| c37 | 122:0.62826 | 24:49.85712 | -307 | 19/09/2014 | 03:25:29 | | | | B |
| c38 | 122:2.49906 | 24:50.35044 | -572 | 19/09/2014 | 06:03:37 | | | | B |
| c39 | 122:2.20578 | 24:50.89254 | -535 | 19/09/2014 | 06:08:35 | | | | B |

Table A1. (Continued)

| No. | longitude (degree:minute) | latitude (degree:minute) | water depth (m) | observation date (dd/mm/yyyy) | observation time (hh:mm:ss) | ship speed (kts) | plume height (m) | tidal type | remark |
|---|---|---|---|---|---|---|---|---|---|
| c40 | 122:2.23211 | 24:51.66115 | -517 | 19/09/2014 | 06:15:47 | 7.4 | 123 | rising | A |
| c41 | 122:2.26786 | 24:51.72484 | -522 | 19/09/2014 | 06:16:21 | 7.4 | 140 | rising | A |
| c42 | 122:2.40032 | 24:51.96696 | -527 | 19/09/2014 | 06:18:31 | 7.4 | 83 | rising | A |
| c43 | 122:2.46990 | 24:52.09873 | -528 | 19/09/2014 | 06:19:41 | 7.4 | 143 | rising | A |
| d01 | 122:27.45384 | 25:12.27260 | -799 | 16/09/2015 | 16:20:47 | 4.6 | 234 | ebb | A |
| d02 | 122:27.17598 | 25:09.72342 | -808 | 17/09/2015 | 07:37:10 | 5.8 | 76 | rising | A |
| d03 | 122:28.92708 | 25:10.83370 | -902 | 17/09/2015 | 07:57:52 | 5 | 246 | rising | A |
| d04 | 122:27.96828 | 25:09.46422 | -938 | 17/09/2015 | 08:39:01 | 6.1 | 291 | rising | A |
| d05 | 122:26.72466 | 25:08.77878 | -930 | 17/09/2015 | 08:52:04 | 5.4 | 258 | rising | A |
| d06 | 122:21.95070 | 25:06.12684 | -932 | 17/09/2015 | 09:41:22 | | | | B |
| d07 | 122:26.79012 | 25:08.02368 | -968 | 17/09/2015 | 15:11:56 | 6.8 | 185 | ebb | A |
| d08 | 122:10.30632 | 24:58.53470 | -610 | 17/09/2015 | 18:50:23 | 6.2 | 158 | low tide | A |
| e01 | 122:13.07700 | 24:55.06990 | -1103 | 21/09/2015 | 09:41:16 | 6.2 | 417 | rising | A |
| e02 | 122:12.67112 | 24:54.90132 | -1072 | 21/09/2015 | 09:45:16 | 6.2 | 368 | rising | A |
| e03 | 122:12.07674 | 24:54.02088 | -1102 | 21/09/2015 | 10:00:16 | 6.4 | 228 | rising | A |
| e04 | 122:35.93888 | 25:03.80614 | -1363 | 21/09/2015 | 22:23:36 | | | | B |
| e05 | 122:35.50185 | 25:03.60770 | -1388 | 21/09/2015 | 22:28:04 | 5.4 | 775 | low tide | A |
| e06 | 122:35.00175 | 25:03.36039 | -1386 | 21/09/2015 | 22:33:20 | 5.4 | 735 | low tide | A |
| e07 | 122:33.45720 | 25:02.60808 | -1400 | 21/09/2015 | 22:48:40 | 6.3 | 809 | low tide | A |
| e08 | 122:34.48506 | 25:04.29324 | -1325 | 21/09/2015 | 23:42:28 | 6 | 328 | low tide | A |
| e09 | 122:34.35660 | 25:08.58780 | -1177 | 22/09/2015 | 05:52:24 | | | | B |
| e10 | 122:33.28500 | 25:12.03930 | -857 | 22/09/2015 | 11:29:56 | 5.9 | 293 | low tide | A |
| e11 | 122:33.24990 | 25:12.27204 | -877 | 22/09/2015 | 12:00:56 | 6.3 | 268 | low tide | A |
| e12 | 122:30.50538 | 25:10.99218 | -916 | 22/09/2015 | 13:53:12 | 6.4 | 466 | rising | A |
| e13 | 122:30.16170 | 25:11.91012 | -881 | 22/09/2015 | 15:27:45 | 5.1 | 184 | rising | A |
| e14 | 122:31.04928 | 25:14.85156 | -790 | 22/09/2015 | 16:24:21 | | | | B |
| f01 | 122:33.37920 | 25:02.73180 | -1825 | 19/04/2016 | 07:32:58 | 6.4 | 997 | rising | A |
| f02 | 122:42.17064 | 24:50.61978 | -1397 | 21/04/2016 | 14:18:39 | 4.8 | 571 | ebb | A |
| f03 | 122:42.06510 | 24:50.77866 | -1348 | 21/04/2016 | 14:55:39 | 5.2 | 668 | ebb | A |
| f04 | 122:42.18024 | 24:51.01878 | -1219 | 21/04/2016 | 14:58:31 | 5.2 | 354 | ebb | A |
| f05 | 122:41.97792 | 24:50.96232 | -1333 | 21/04/2016 | 18:50:31 | 5.2 | 610 | rising | A |
| f06 | 122:41.86212 | 24:51.09972 | -1302 | 21/04/2016 | 19:17:51 | 5.3 | 608 | rising | A |
| g01 | 122:33.62808 | 25:02.99238 | -1382.00 | 26/04/2016 | 06:31:35.6 | 8.3 | 212 | low tide | A |
| h01 | 122:42.04206 | 24:50.83140 | -1375 | 05/05/2016 | 13:18:11 | 12 | 647 | ebb | A |
| h02 | 122:43.16988 | 24:58.69440 | -1498 | 06/05/2016 | 17:05:40 | 6.2 | 660 | rising | A |
| h03 | 122:42.97428 | 24:58.69782 | -1500 | 06/05/2016 | 21:01:40 | 5.8 | 328 | rising | A |
| h04 | 122:42.82872 | 24:58.79136 | -1481 | 05/06/2016 | 21:37:07 | | | | B |
| h05 | 122:41.98362 | 24:58.58502 | -1491 | 07/05/2016 | 06:49:28 | 5.5 | 460 | rising | A |
| h06 | 122:37.59948 | 24:48.97866 | -1338 | 07/05/2016 | 08:34:36 | 5.9 | 299 | rising | A |
| h07 | 122:37.41108 | 24:48.92952 | -1334 | 07/05/2016 | 08:55:04 | 5.9 | 140 | rising | A |
| h08 | 122:37.95426 | 24:50.12514 | -1447 | 07/05/2016 | 09:08:12 | | | | B |
| h09 | 122:41.77320 | 24:58.54824 | -1488 | 07/05/2016 | 10:40:16 | 5.9 | 415 | rising | A |
| h10 | 122:37.84356 | 24:50.26794 | -1449 | 07/05/2016 | 12:56:12 | | | | B |
| h11 | 122:37.29138 | 24:49.02384 | -1340 | 07/05/2016 | 13:10:28 | | | | B |
| h12 | 122:36.85944 | 24:48.06066 | -1274 | 07/05/2016 | 13:21:20 | 5.2 | 541 | ebb | A |
| h13 | 122:37.64544 | 24:50.20494 | -1457 | 07/05/2016 | 13:47:40 | | | | B |
| h14 | 122:37.46962 | 24:50.16793 | -1461 | 07/05/2016 | 17:20:04 | 5.5 | 452 | rising | A |
| h15 | 122:37.41507 | 24:50.05328 | -1442 | 07/05/2016 | 17:21:20 | 5.5 | 400 | rising | A |
| h16 | 122:37.38773 | 24:49.98682 | -1428 | 07/05/2016 | 17:22:04 | 5.5 | 352 | rising | A |
| h17 | 122:36.62244 | 24:48.28260 | -1292 | 07/05/2016 | 17:41:00 | 5.9 | 203 | rising | A |

Table A1. (Continued)

| No. | longitude (degree:minute) | latitude (degree:minute) | water depth (m) | observation date (dd/mm/yyyy) | observation time (hh:mm:ss) | ship speed (kts) | plume height (m) | tidal type | remark |
|---|---|---|---|---|---|---|---|---|---|
| h18 | 122:36.46548 | 24:48.24186 | -1287 | 07/05/2016 | 17:49:36 | 5.6 | 545 | rising | A |
| h19 | 122:37.22454 | 24:50.02332 | -1440 | 07/05/2016 | 18:08:48 | 5.4 | 776 | | A |
| h20 | 122:40.20090 | 24:57.11874 | -1405 | 07/05/2016 | 20:32:12 | 5.8 | 384 | rising | A |
| h21 | 122:37.43281 | 24:50.83457 | -1490 | 07/05/2016 | 21:40:36 | 5.8 | 843 | rising | A |
| h22 | 122:37.34504 | 24:50.63361 | -1488 | 07/05/2016 | 21:42:56 | 5.8 | 805 | rising | A |
| h23 | 122:37.25904 | 24:50.44596 | -1482 | 07/05/2016 | 21:45:08 | 5.8 | 833 | rising | A |
| h24 | 122:37.16016 | 24:50.23662 | -1465 | 07/05/2016 | 21:47:40 | 5.8 | 831 | rising | A |
| h25 | 122:37.01454 | 24:50.23770 | -1466 | 07/05/2016 | 22:44:24 | 5.8 | 739 | high tide | A |
| h26 | 122:37.17618 | 24:50.62746 | -1487 | 07/05/2016 | 22:48:52 | 5.8 | 771 | high tide | A |
| h27 | 122:39.99144 | 24:57.05250 | -1384 | 08/05/2016 | 00:00:00 | | | | B |
| h28 | 122:39.83514 | 24:57.15108 | -1402 | 08/05/2016 | 01:12:08 | | | | B |
| h29 | 122:37.11696 | 24:50.82839 | -1495 | 08/05/2016 | 02:25:04 | 6.2 | 791 | ebb | A |
| h30 | 122:36.87783 | 24:50.32349 | -1481 | 08/05/2016 | 02:31:52 | 6.2 | 715 | ebb | A |
| h31 | 122:36.58740 | 24:50.03958 | -1417 | 08/05/2016 | 03:30:12 | 5.8 | 291 | ebb | A |
| h32 | 122:36.92208 | 24:50.80584 | -1506 | 08/05/2016 | 03:38:32 | 5.8 | 548 | ebb | A |
| h33 | 122:36.76464 | 24:52.86552 | -1515 | 08/05/2016 | 17:26:20 | 6.1 | 537 | low tide | A |
| h34 | 122:36.72912 | 24:53.17368 | -1516 | 08/05/2016 | 20:02:08 | 5.6 | 934 | rising | A |
| h35 | 122:36.53694 | 24:53.13180 | -1515 | 08/05/2016 | 21:32:04 | 5.6 | 685 | rising | A |
| h36 | 122:15.91903 | 25:02.87999 | -776 | 09/05/2016 | 02:30:56 | | | | B |
| h37 | 122:15.72340 | 25:02.95878 | -715 | 09/05/2016 | 02:32:12 | | | | B |
| h38 | 122:15.58939 | 25:03.01194 | -659 | 09/05/2016 | 02:33:04 | | | | B |
| i01 | 122:36.56627 | 24:53.23438 | -1513 | 07/04/2017 | 07:35:02 | 4.9 | 922 | rising | A |
| i02 | 122:36.84848 | 24:53.06042 | -1514 | 07/04/2017 | 07:37:47 | 4.9 | 771 | rising | A |
| i03 | 122:37.50606 | 24:50.19276 | -1460 | 07/04/2017 | 08:41:11 | 6.9 | 726 | ebb | A |
| i04 | 122:37.19286 | 24:50.37870 | -1477 | 07/04/2017 | 08:44:24 | 6.9 | 855 | ebb | A |
| i05 | 122:41.97390 | 25:06.93762 | -1385 | 07/04/2017 | 13:52:12 | 6.0 | 971 | ebb | A |
| i09 | 122:32.54004 | 24:54.13110 | -1187 | 10/04/2017 | 13:25:25 | 6.5 | 220 | ebb | A |
| i10 | 122:32.31738 | 24:54.14604 | -1303 | 10/04/2017 | 16:13:46 | 6.4 | 724 | low tide | A |
| i11 | 122:35.61846 | 25:03.45132 | -1377 | 11/04/2017 | 01:58:19 | 5.9 | 602 | ebb | A |
| i12 | 122:35.76450 | 25:03.80796 | -1373 | 11/04/2017 | 02:01:50 | 5.9 | 624 | ebb | A |
| i13 | 122:35.79810 | 25:03.90120 | -1372 | 11/04/2017 | 02:02:41 | 5.9 | 355 | ebb | A |
| i14 | 122:35.66838 | 25:04.15384 | -1380 | 11/04/2017 | 03:59:27 | 5.7 | 605 | ebb | A |
| i15 | 122:35.61835 | 25:04.02019 | -1373 | 11/04/2017 | 04:00:48 | 5.7 | 209 | ebb | A |
| i16 | 122:35.55865 | 25:03.87180 | -1374 | 11/04/2017 | 04:02:18 | 5.7 | 301 | ebb | A |
| i17 | 122:35.46471 | 25:03.64079 | -1388 | 11/04/2017 | 04:04:43 | 5.7 | 655 | ebb | A |
| i18 | 122:35.12118 | 25:03.39624 | -1387 | 11/04/2017 | 10:17:06 | 5.4 | 155 | rising | A |
| i19 | 122:35.25898 | 25:03.72546 | -1381 | 11/04/2017 | 10:20:42 | 5.4 | 651 | rising | A |
| i20 | 122:35.40202 | 25:04.10702 | -1387 | 11/04/2017 | 10:25:07 | 5.4 | 522 | rising | A |
| i21 | 122:35.06496 | 25:03.81289 | -1326 | 11/04/2017 | 12:42:00 | 6.6 | 314 | ebb | A |
| i22 | 122:34.94747 | 25:03.51430 | -1369 | 11/04/2017 | 12:45:21 | 6.6 | 761 | ebb | A |
| i23 | 122:32.53968 | 24:57.50520 | -1487 | 11/04/2017 | 13:52:30 | 5.7 | 530 | ebb | A |
| i24 | 122:32.49528 | 24:57.38904 | -1489 | 11/04/2017 | 13:53:42 | 5.7 | 794 | ebb | A |
| i25 | 122:32.32482 | 24:57.54444 | -1489 | 11/04/2017 | 18:32:37 | 6.2 | 952 | rising | A |
| i26 | 122:34.72758 | 25:03.55866 | -1362 | 11/04/2017 | 19:54:49 | 4.9 | 948 | rising | A |
| i27 | 122:34.79928 | 25:04.29942 | -1329 | 11/04/2017 | 22:30:33 | 5.2 | 726 | rising | A |
| i28 | 122:22.75344 | 24:55.27152 | -1314 | 12/04/2017 | 04:22:16 | 8.9 | 356 | ebb | A |
| j01 | 122:34.54716 | 25:04.27806 | -1323 | 13/04/2017 | 10:17:32 | 8.9 | 250 | rising | A |
| j02 | 122:33.57534 | 25:02.42076 | -1401 | 13/04/2017 | 12:42:40 | 5.2 | 360 | high tide | A |
| j03 | 122:33.32256 | 25:01.80990 | -1411 | 13/04/2017 | 12:49:40 | 5.2 | 350 | high tide | A |
| j04 | 122:33.08934 | 25:01.77259 | -1410 | 13/04/2017 | 18:38:11 | 6.4 | 285 | rising | A |

Table A1. (Continued)

| No. | longitude (degree:minute) | latitude (degree:minute) | water depth (m) | observation date (dd/mm/yyyy) | observation time (hh:mm:ss) | ship speed (kts) | plume height (m) | tidal type | remark |
|---|---|---|---|---|---|---|---|---|---|
| j05 | 122:33.36570 | 25:02.45893 | -1404 | 13/04/2017 | 18:56:19 | 6.8 | 990 | rising | A |
| j06 | 122:33.39529 | 25:02.53489 | -1402 | 13/04/2017 | 18:58:51 | 6.8 | 706 | rising | A |
| j07 | 122:33.28068 | 25:02.83188 | -1396 | 13/04/2017 | 21:35:35 | | | | B |
| j08 | 122:35.12502 | 25:07.99194 | -1207 | 14/04/2017 | 04:59:39 | 5.4 | 320 | ebb | A |
| j09 | 122:29.79868 | 24:55.11381 | -1390 | 14/04/2017 | 08:02:27 | 6.3 | 388 | rising | A |
| j10 | 122:34.46501 | 25:08.46681 | -1165 | 15/04/2017 | 15:30:37 | | | | B |
| j11 | 122:34.01034 | 25:07.85514 | -1180 | 15/04/2017 | 16:09:25 | 5.8 | 611 | ebb | A |
| j12 | 122:33.80892 | 25:07.82325 | -1150 | 16/04/2017 | 00:11:49 | | | | B |
| j13 | 122:33.71219 | 25:08.08471 | -1110 | 16/04/2017 | 00:54:53 | 5.5 | 168 | high tide | A |
| j14 | 122:32.18146 | 25:05.27541 | -1298 | 16/04/2017 | 10:39:25 | 6.4 | 818 | rising | A |
| j15 | 122:32.13055 | 25:05.14374 | -1307 | 16/04/2017 | 10:40:49 | 6.4 | 575 | rising | A |
| j16 | 122:31.63586 | 25:04.45576 | -1273 | 16/04/2017 | 18:03:09 | 5.8 | 475 | ebb | A |
| j17 | 122:31.97088 | 25:05.79804 | -1223 | 16/04/2017 | 19:47:49 | 6.5 | 502 | low tide | A |
| j18 | 122:31.76810 | 25:05.87408 | -1174 | 17/04/2017 | 01:17:09 | | | | B |
| j19 | 122:34.00046 | 25:10.38862 | -939 | 17/04/2017 | 05:02:54 | | | | B |
| j20 | 122:33.96796 | 25:10.30323 | -969 | 17/04/2017 | 05:03:54 | | | | B |
| j21 | 122:34.29048 | 25:10.03050 | -992 | 17/04/2017 | 05:30:46 | 5.8 | 286 | ebb | A |
| k01 | 121:51.08244 | 25:10.64736 | 104 | 14/03/2018 | 03:57:19 | 5.1 | 97 | ebb | A |
| k02 | 122:10.69314 | 24:47.34618 | 223 | 14/03/2018 | 09:16:01 | 4.9 | 88 | high tide to ebb | A |
| k03 | 122:14.68548 | 24:48.11568 | 795 | 14/03/2018 | 11:33:54 | | | | B |
| k04 | 122:14.92976 | 24:47.87954 | 700 | 14/03/2018 | 14:10:38 | 6.3 | 104 | ebb | A |
| k0S | 122:15.10925 | 24:48.39673 | 794 | 14/03/2018 | 14:16:08 | 6.3 | 157 | ebb | A |
| k06 | 122:15.18323 | 24:48.62531 | 855 | 14/03/2018 | 14:18:32 | 6.3 | 114 | ebb | A |
| k07 | 122:15.92268 | 24:so.72676 | 1462 | 14/03/2018 | 14:40:41 | | | | B |
| k08 | 122:16.54356 | 24:52.50714 | 398 | 14/03/2018 | 15:00:05 | 6 | 224 | low tide | A |
| k09 | 122:15.38660 | 24:48.74790 | 905 | 14/03/2018 | 19:45:35 | | | | B |
| k10 | 122:15.30876 | 24:48.48746 | 834 | 14/03/2018 | 19:48:53 | | | | B |
| k11 | 122:15.16673 | 24:48.12952 | 719 | 14/03/2018 | 19:53:36 | 4.8 | 104 | rising | A |
| k12 | 122:15.52032 | 24:48.62100 | 923 | 14/03/2018 | 22:24:18 | 5 | 205 | high tide to ebb | A |
| k13 | 122:21.86868 | 25:06.35471 | 888 | 15/03/2018 | 01:51:09 | 4.6 | 235 | ebb | A |
| k14 | 122:21.89781 | 25:06.41817 | 853 | 15/03/2018 | 01:51:54 | 4.6 | 198 | ebb | A |
| k1S | 122:22.00404 | 25:06.28512 | 908 | 15/03/2018 | 02:01:30 | 4.5 | 267 | ebb | A |
| k16 | 122:15.70200 | 24:48.64770 | 903 | 15/03/2018 | 05:25:52 | 6.2 | 215 | rising | A |
| k17 | 122:23.21718 | 25:08.68632 | 788 | 15/03/2018 | 13:18:53 | 5.4 | 258 | ebb | A |
| k18 | 122:17.14644 | 24:51.78942 | 1151 | 15/03/2018 | 16:27:04 | | | | B |
| k19 | 122:15.51900 | 24:47.24934 | 711 | 15/03/2018 | 17:18:58 | 5.2 | 86 | rising | A |
| k20 | 122:23.39412 | 25:08.12904 | 911 | 15/03/2018 | 23:14:10 | 5.9 | 253 | high tide to ebb | A |
| k21 | 122:17.04258 | 24:48.60810 | 976 | 16/03/2018 | 07:44:07 | 4.6 | 271 | rising | A |
| k22 | 122:17.45004 | 24:45.46896 | 760 | 19/03/2018 | 15:17:16 | 5.9 | 160 | ebb | A |
| k23 | 122:20.27982 | 24:53.09664 | 1116 | 18/03/2018 | 16:44:37 | 5.8 | 520 | ebb | A |
| k24 | 122:27.37884 | 25:12.14142 | 770 | 18/03/2018 | 20:19:49 | | | | B |
| k25 | 122:26.61870 | 25:08.81052 | 932 | 18/03/2018 | 21:01:37 | | | | B |
| k26 | 122:26.58204 | 25:08.70516 | 938 | 18/03/2018 | 21:02:46 | | | | B |
| k27 | 122:20.69670 | 24:52.91262 | 1188 | 19/03/2018 | 00:06:06 | | | | B |
| k28 | 122:18.86118 | 24:47.94852 | 810 | 19/03/2018 | 01:04:27 | | | | B |
| k29 | 122:17.94060 | 24:45.43818 | 804 | 19/03/2018 | 01:32:35 | 5.4 | 154 | ebb | A |
| k30 | 122:21.27000 | 24:53.03172 | 1204 | 19/03/2018 | 03:56:51 | | | | B |
| k31 | 122:21.96660 | 24:54.90984 | 1364 | 19/03/2018 | 04:18:38 | | | | B |
| k32 | 122:26.82264 | 25:08.01192 | 977 | 19/03/2018 | 06:52:31 | 5.3 | 460 | rising | A |
| k33 | 122:27.90834 | 25:09.49254 | 943 | 19/03/2018 | 08:15:58 | 6.4 | 260 | rising | A |

Table A1. (Continued)

| No. | longitude (degree:minute) | latitude (degree:minute) | water depth (m) | observation date (dd/mm/yyyy) | observation time (hh:mm:ss) | ship speed (kts) | plume height (m) | tidal type | remark |
|---|---|---|---|---|---|---|---|---|---|
| l01 | 122:22.58058 | 24:55.19514 | 1316 | 22/03/2018 | 10:57:08 | | | | B |
| l02 | 122:27.38316 | 25:66.62448 | 1055 | 22/03/2018 | 13:29:49 | | | | B |
| l03 | 122:28.93146 | 25:10.84356 | 912 | 22/03/2018 | 14:17:41 | 5.4 | 156 | high tide | A |
| l04 | 122:28.96914 | 25:10.95924 | 907 | 22/03/2018 | 14:18:55 | 5.4 | 237 | high tide | A |
| l05 | 122:21.79782 | 24:53.01264 | 1233 | 22/03/2018 | 22:08:47 | 5.4 | 535 | rising | A |
| l06 | 122:22.58346 | 24:48.83064 | 1113 | 23/03/2018 | 10:56:08 | 6.1 | 195 | rising | A |
| l07 | 122:23.11652 | 24:48.55148 | 1178 | 23/03/2018 | 12:52:20 | | | | B |
| l08 | 122:23.25352 | 24:48.92977 | 1163 | 23/03/2018 | 12:56:32 | | | | B |
| l09 | 122:23.38523 | 24:49.24968 | 1166 | 23/03/2018 | 13:00:11 | 5.5 | 630 | rising | A |
| l10 | 122:23.48298 | 24:49.54314 | 1204 | 23/03/2018 | 13:03:26 | | | | B |
| l11 | 122:23.51394 | 24:49.62876 | 1263 | 23/03/2018 | 13:04:23 | 5.5 | 265 | rising | A |
| l12 | 122:33.13134 | 25:12.28986 | 891 | 24/03/2018 | 05:11:10 | | | | B |
| l13 | 122:33.37064 | 25:12.12494 | 865 | 24/03/2018 | 05:20:10 | 5.6 | 135 | ebb | A |
| l14 | 122:33.30584 | 25:11.92467 | 896 | 24/03/2018 | 05:22:28 | | | | B |
| l15 | 122:25.22646 | 24:50.06544 | 1310 | 24/03/2018 | 09:25:47 | 5.7 | 465 | low tide | A |
| l16 | 122:18.99276 | 24:46.81308 | 872 | 24/03/2018 | 11:38:26 | 6 | 136 | rising | A |
| l17 | 122:29.75856 | 24:55.05750 | 1284 | 25/03/2018 | 00:23:56 | 4.2 | 780 | rising | A |
| m01 | 122:34.96194 | 25:03.48648 | -1366 | 04/05/2018 | 06:13:19 | 11.1 | 855 | ebb | A |
| m02 | 122:35.47140 | 25:03.60918 | -1380 | 04/05/2018 | 06:16:07 | 11.1 | 879 | ebb | A |
| m03 | 122:32.58720 | 24:54.07938 | -1133 | 09/05/2018 | 09:03:58 | 7.1 | 218 | ebb | A |
| m04 | 122:32.46246 | 24:54.17898 | -1202 | 09/05/2018 | 15:29:19 | 2.7 | 335 | rising | A |
| mo5 | 122:35.46742 | 25:03.47854 | -1370 | 11/05/2018 | 01:16:31 | 7.9 | 576 | low tide | A |
| m06 | 122:35.10787 | 25:03.64018 | -1267 | 11/05/2018 | 01:21:46 | 7.9 | 635 | low tide | A |
| m07 | 122:34.84143 | 25:03.70536 | -1235 | 11/05/2018 | 01:24:13 | 7.9 | 410 | low tide | A |